A simple control-oriented model of an indirect-fired strip annealing furnace

authored by **M. Niederer, S. Strommer, A. Steinboeck, and A. Kugi**

and published in *International Journal of Heat and Mass Transfer*.

Cite this article as:

M. Niederer, S. Strommer, A. Steinboeck, and A. Kugi, "A simple control-oriented model of an indirect-fired strip annealing furnace", *International Journal of Heat and Mass Transfer*, vol. 78, pp. 557–570, 2014. DOI: 10.1016/j.ijheatmasstransfer.2014.06.080

BibTex entry:

```
@ARTICLE{acinpaper,
  AUTHOR = {Niederer, M. and Strommer, S. and Steinboeck, A. and Kugi, A.},
  TITLE = {A simple control-oriented model of an indirect-fired strip annealing furnace},
  JOURNAL = {International Journal of Heat and Mass Transfer},
  YEAR = {2014},
  volume = {78},
  pages = {557-570},
  doi = {10.1016/j.ijheatmasstransfer.2014.06.080},
  url = {http://www.sciencedirect.com/science/article/pii/S0017931014005523}
}
```

Link to original paper:

http://dx.doi.org/10.1016/j.ijheatmasstransfer.2014.06.080
http://www.sciencedirect.com/science/article/pii/S0017931014005523

Contact:

Automation and Control Institute (ACIN)
Vienna University of Technology
Gusshausstrasse 27-29/E376
1040 Vienna, Austria

Internet: www.acin.tuwien.ac.at
E-mail: office@acin.tuwien.ac.at
Phone: +43 1 58801 37601
Fax: +43 1 58801 37699

A simple control-oriented model of an indirect-fired strip annealing furnace

M. Niederer*, S. Strommer, A. Steinboeck, A. Kugi

Automation and Control Institute, Vienna University of Technology, Gußhausstraße 27–29, 1040 Vienna, Austria

Abstract

A simple mathematical model of an indirect-fired strip annealing furnace for real-time control and optimization purposes is developed. The considered furnace is part of a hot-dip galvanizing line and is used for continuous heat treatment of steel strips. The heat that is released during the combustion process inside the radiant tubes is calculated by means of steady-state mass and enthalpy balances. For discretizing the heat conduction problem of the radiant tube wall and the furnace wall, Galerkin's method is used. Furthermore, simple heat balances are employed to model the temperature evolution of the guiding rolls and the strip. To facilitate an accurate representation of the strip temperature, the strip motion is described by Lagrangian coordinates. Heat transfer by conduction and radiation interconnects the individual dynamic submodels. Measurements from the real plant demonstrate the accuracy of the derived model, which is computationally rather inexpensive and thus suitable for model-based control and optimization.

Key words: Steel industry, annealing furnace, indirect-fired furnace, radiant tube, Lagrangian coordinates, radiative heat transfer, net-radiation method

1. Introduction

1.1. Strip annealing furnaces

In the steel industry, annealing furnaces are used for reheating and heat treatment of steel products. The annealing furnace considered in this analysis is part of a hot-dip galvanizing line of voestalpine Stahl GmbH in Linz, Austria. In this strip processing line, a combined direct- and indirect-fired furnace is installed for the heat treatment of steel strip in order to achieve the desired material properties and to prepare the strips for subsequent surface treatment, i.e., hot dip galvanizing. In this paper, the indirect-fired furnace that comes right after the direct-fired furnace [43] will be addressed. To realize a continuous operation of this processing line, the strips are welded together to form an endless strip.

1.2. Motivation for a furnace model

The heat treatment of steel strips consumes large amounts of energy. For a high product quality, the temperature evolution of the strip processed in the furnace is of vital importance. In order to achieve the desired product properties, the strip has to be heated according to a predefined temperature trajectory [3, 7]. From a control point of view, this is a challenging task, particularly in transient furnace operation, e.g., when a welded joint traverses the furnace or when the strip velocity changes. The control task is further complicated by the fact that the strip temperature can only be monitored by radiation pyrometers located at a very few discrete points in the furnace. Since the demands on the furnace operation in terms of product quality, energy consumption, and flue gas emissions are steadily increasing, there is a need for advanced control and optimization methods that take into account all these difficulties.

In the current paper, a mathematical model of the indirect-fired strip annealing furnace is derived. The focus of research is to obtain a dynamical model of the strip temperature that captures the essential nonlinearities of the system and that is a good compromise between accuracy and computational efficiency. In fact, the model should be real-time capable. The proposed model should serve as a point of departure for designing a model-based control concept for the considered furnace.

1.3. Indirect-fired furnace

The considered indirect-fired furnace, schematically shown in Fig. 1, consists of a radiant tube heating section (RTH) and a radiant tube soaking section (RTS) which are separated by a partition wall. Both sections are equipped with W-shaped radiant tubes that are grouped into individual control zones. All radiant tubes of a control zone are supplied with the same amount of fuel and combustion air. Moreover, the radiant tubes are controlled in a continuous mode meaning that the fuel supply can be adjusted continuously between a minimum and maximum value.

Inside each radiant tube, natural gas is burnt in a fuel-lean combustion process. The heat released by the combustion process is either transferred through the wall of the radiant tube into the furnace chamber or it is lost in form of sensible heat of the exhaust gas leaving the radiant tube after a local recuperator, which is used for preheating the combustion air. Within the furnace chamber, the supplied heat is used for heating the strip

*Corresponding author. *Tel.:* +43 1 58801 376292, *fax:* +43 1 58801 9376264.

Email address: niederer@acin.tuwien.ac.at (M. Niederer)

Preprint submitted to International Journal of Heat and Mass Transfer *August 4, 2014*

Post-print version of the article: M. Niederer, S. Strommer, A. Steinboeck, and A. Kugi, "A simple control-oriented model of an indirect-fired strip annealing furnace", *International Journal of Heat and Mass Transfer*, vol. 78, pp. 557–570, 2014. doi: 10.1016/j.ijheatmasstransfer.2014.06.080

Nomenclature

Latin symbols

$\mathbf{B}$	vector of radiosities (W/m^2)
B_i	radiosity (W/m^2)
b_s	strip width (m)
c_i	specific heat capacity (J/kg K)
D_r	diameter of a radiant tube (m)
d_i	thickness (m)
g_i	weighting factor (–)
$\mathbf{H}_i$	vector of irradiances (W/m^2)
H_i	irradiance (W/m^2)
h	specific enthalpy per mol (J/mol)
$\Delta\bar{h}^0$	enthalpy of reaction per mol (J/mol)
Δh^0	enthalpy of reaction per kg (J/kg)
$h_i(y)$	trial function (–)
i	index
J	number of layers of the wall
j	index
K_1	constant of lumped parameter system of the wall (J/m^{2}K)
K_2	constant of lumped parameter system of the wall (W/m^{2}K)
k_i	thermal heat conductivity (W/mK)
L	length of a tube (m)
$\mathbf{M}$	mapping matrix (–)
M_i	molar mass (kg/mol)
$\dot{m}_i$	mass flow (kg/s)
N_d	number of deflection rolls
N_G	number of trial functions
N_r	number of radiant tubes
N_s	number of strip elements (Eulerian framework)
$N_{\tilde{s}}$	number of strip elements (Lagrangian framework)
N_w	number of wall sections
N_z	number of control zones
$\mathbf{P}$	matrix for computing heat flux densities (W/m^{2}K^4)
$\dot{Q}_i$	heat flow (W)
$\dot{\mathbf{q}}_i$	vector of heat flux densities (W/m^2)
$\dot{q}_i$	heat flux density (W/m^2)
R_c	thermal contact resistance
r_{ij}	distance between two interacting surfaces (m)
$\mathbf{S}$	vector of surface areas (m^2)
S_i	surface area (m^2)
$\overline{\mathbf{ss}}$	matrix of direct exchange areas (m^2)
$\overline{s_i s_j}$	direct exchange area (m^2)
$\mathbf{T}_i$	vector of temperatures (K)
T_i	either temperature or Galerkin coefficient (K)
T_o	outer surface temperature of the wall (K)
t	time (s)
t_k	sampling instant (s)
$\mathbf{u}_i$	vector of input quantities, either (kg/s) or (K)
v_s	strip velocity (m/s)
x, y, z	Eulerian coordinates (m)
$\tilde{x}, \tilde{y}, \tilde{z}$	Lagrangian coordinates (m)

Greek symbols

Δt_k	sampling period (s)
$\boldsymbol{\varepsilon}_i$	vector of emissivities (–)
ε_i	emissivity (–)
$\boldsymbol{\Gamma}_i$	mapping matrix (–)
λ	excess air coefficient (–)
ρ_i	mass density (kg/m^3)
σ	Stefan-Boltzmann constant (W/m^{2}K^4)
Θ	temperature field (K)
θ_i	angle of incidence (rad)

Operators

$\mathcal{B}_j^{\mp}$	(differential) operator of boundary condition (W/m^2) or (K)
$\mathcal{D}_j$	differential operator of heat conduction equation (W/m^3)

Subscripts

c	combustion
d	deflection roll
r	radiant tube
s	strip
w	wall

Superscripts

c	conduction

Symbols on top of variables

$\tilde{}$	Lagrangian framework

and the furnace or at least for keeping their temperatures at a desired level.

The strip is preheated in the direct-fired furnace and enters the indirect-fired furnace at an air lock that separates these two furnaces. Inside the indirect-fired furnace, the strip is conveyed through the furnace along a meander-shaped path by means of deflection rolls. The next processing step after the furnace is a cooling section. In the furnace, the strip is mainly heated by thermal radiation, which is the dominant mechanism of heat transfer in such furnaces [5, 14, 45]. Furthermore, to prevent the strip from oxidation, an inert gas atmosphere is realized inside the furnace.

The heat that is transferred into the furnace chamber but not used for heating the strip, leaves the furnace through the furnace wall. To keep this heat loss low, the casing of the furnace consists of well-insulating refractory material.

Post-print version of the article: M. Niederer, S. Strommer, A. Steinboeck, and A. Kugi, "A simple control-oriented model of an indirect-fired strip annealing furnace", *International Journal of Heat and Mass Transfer*, vol. 78, pp. 557–570, 2014. DOI: 10.1016/j.ijheatmasstransfer.2014.06.080
The content of this post-print version is identical to the published paper but without the publisher's final layout or copy editing.

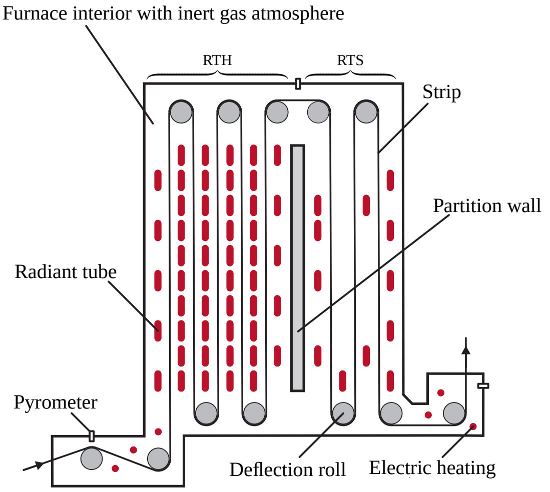

Figure 1: Indirect-fired strip annealing furnace.

1.4. Existing furnace models

Due to the large number of publications on modeling indirect-fired furnaces and their components, this literature overview can only serve as a starting point for an in-depth exploration. One way to describe the physical phenomena inside the furnace as precise as possible are expensive numerical methods [6, 9, 11], e.g., the finite element method or computational fluid dynamics simulations. Numerical methods are commonly used for designing new furnaces and for off-line studies. Usually, the mathematical complexity and dimension of such models is very high and for this reason they are not suitable for control and real-time optimization methods.

For industrial control applications, usually simpler mathematical models based on physical or empirical correlations are used. A disadvantage of empirical correlations is that they do not allow a direct physical interpretation. However, if the real physical structure is unknown, this approach may be a better choice than first-principles models. Some models for furnace control, based on both fundamental theory of thermodynamics and empirically determined furnace behavior, are presented in [22, 28, 45, 48].

Inside an indirect-fired strip annealing furnace, the strip is mainly heated by radiant tubes. In [1, 36, 37], different radiant tube models that capture real physical effects, i.e., the combustion and the heat conduction, are presented. However, due to their mathematical complexity, these are in conflict with the afore mentioned requirements for the furnace model.

Most frequently, the heat conduction problem in the furnace is solved by means of the finite difference method, e.g., [8, 11, 26, 29, 32, 36]. This method yields a set of ordinary differential equations. The number of equations depends on the spatial discretization. An alternative approach would be the weighted residual method [12, 13, 50], which is addressed in Sec. 2.1.

Many published furnace models, e.g., [8, 25, 26], consider the strip temperature in form of a simple heat balance in an Eulerian coordinate system. For an exact representation of the strip temperature, this approach requires a relatively fine discretization of the strip along the furnace. The alternative Lagrangian coordinate system, i.e., material fixed, is utilized in this paper.

Another distinguishing factor of the different furnace models is the formal representation of the heat exchange mechanism in the furnace. Most models take into account some form of radiative heat exchange [11, 26, 33, 36, 48]. The level of detail ranges from the simple consideration of the Stefan-Boltzmann law to the consideration of the coupling behavior of the radiative heat exchange, i.e., the entire furnace geometry is taken into account. Generally, the calculation of radiative heat transfer requires the determination of so-called direct-exchange areas, which describe the geometric relation between surface sections in the furnace. Since this is a laborious task, in particular for 3-dimensional scenarios, usually 2-dimensional furnace geometries are assumed.

Indirect-fired strip annealing furnaces are complex dynamical systems. Although there exist several models for this type of furnaces, they cannot be directly applied to the considered furnace, because hardly any furnace is a duplicate, i.e., they differ significantly with respect to design and processed products. Moreover, most published models use some simplifying assumptions, e.g., neglecting the coupling behavior of thermal radiation, which may limit the accuracy of the derived model. Since the focus of this research is to obtain an accurate and computationally inexpensive mathematical model for control and optimization of the considered indirect-fired furnace, a tailored model is derived.

A tailored mathematical model was also derived for the direct-fired furnace of the considered hot-dip galvanizing line and reported in [43]. The following explains why this model is not directly transferable to the indirect-fired furnace analyzed here: In the direct-fired furnace, the strip is heated by the hot flue gas which streams in the opposite direction of the strip, i.e., the flue gas is in direct contact with the strip. To avoid oxidation of the strip, the fuel is burnt in a fuel-rich combustion process. Furthermore, the flue gas is participating in the radiative heat exchange process. In contrast, in the indirect-fired furnace the fuel is burnt in a fuel-lean combustion process inside the radiant tubes and the strip itself is surrounded by inert gas, which is transparent for thermal radiation and which prevents oxidation of the product surface. For this reason, the temperature evolution of the strip is mainly controlled by the surface temperatures of the radiant tubes. This demands the thermal modeling of the radiant tubes including the burner and the recuperator. Furthermore, semi-empirical approximations for a tunnel-like shape with rectangular cross section are used for calculating the radiative heat exchange in the direct-fired furnace. This simplifying modeling approach cannot be used for the indirect-fired furnace, where the strip moves along a meander-like path through a big furnace chamber, cf. Fig. 1. This configuration entails multiple radiative interactions between different strip sections. To capture this dynamic coupling effect by the mathematical model, the full 3-dimensional geometry is taken into account for the radiation analysis presented in this paper.

Post-print version of the article: M. Niederer, S. Strommer, A. Steinboeck, and A. Kugi, “A simple control-oriented model of an indirect-fired strip annealing furnace”, *International Journal of Heat and Mass Transfer*, vol. 78, pp. 557–570, 2014. DOI: 10.1016/j.ijheatmasstransfer.2014.06.080

1.5. Contents

The paper is structured as follows: In Sec. 2, the mathematical model of the considered indirect-fired strip annealing furnace is derived based on first principles. The continuous-time state space model finally consists of the submodels for the furnace wall, the radiant tubes, the strip, and the deflection rolls. The thermal interaction of these submodels is described by means of the heat transfer mechanisms radiation and conduction. Moreover, an explicit time integration scheme is proposed for discretizing the time domain, as required for computer implementation. The discretization error entailed by the numerical solution of the model is investigated by means of a grid convergence study. In Sec. 3, the accuracy of the derived furnace model is verified by a comparison of simulation results with measurement data from the real plant. Finally, Sec. 4 contains some conclusions. Throughout the paper, an attempt is made to provide at least the most fundamental equations necessary to review and utilize the proposed modeling method.

2. Mathematical model

2.1. Wall

This section deals with the heat conduction problem of the multi-layered furnace wall. The individual layers of the wall have different material properties, which should be taken into account by the model. Many authors (cf. [34, 44]) use the finite difference method for discretizing the spatial domain of such a problem. However, here the Galerkin method is applied to obtain a low dimensional model that is computationally efficient.

2.1.1. Heat conduction problem

Let $\Theta_{w,i}(y,t) > 0$ be the temperature field in a section i, where $i = 1, \dots, N_w$, of a multi-layered furnace wall defined along the spatial direction y. The extension of the wall in y-direction corresponds to the range $[0, d_w]$ as shown in Fig. 2. Since the temperature gradient along y is generally significantly larger than in a plane parallel to the wall, a 1-dimensional heat conduction is a reasonable approximation.

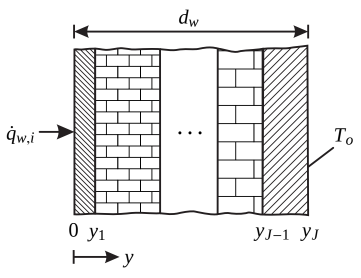

Figure 2: Section of a multi-layered furnace wall.

A typical wall of the indirect-fired furnace (cf. Fig. 2) consists of a casing (outside), several insulation layers, and a cladding, which is an additional thin layer at the inner surface of the furnace. A single layer j is characterized by its thickness $d_{w,j} = y_j - y_{j-1}$ and its material parameters, i.e., the specific heat capacity $c_{w,j}$, the mass density $\rho_{w,j}$, and the heat conductivity $k_{w,j}$. In general, these material parameters are temperature-dependent. J is the number of layers, so that $j = 1, \dots, J$. Within each layer, the material is assumed to be homogeneous.

The heat flux through the furnace wall is determined by the material properties of the individual layers, the temperature gradient inside the solid, and the boundary conditions at $y = 0$ and $y = d_w$. Using the operators

$$\mathcal{D}(\Theta_{w,i}) := \rho_w(y) c_w(y, \Theta_{w,i}) \frac{\partial \Theta_{w,i}}{\partial t} - \frac{\partial}{\partial y}\left(k_w(y, \Theta_{w,i}) \frac{\partial \Theta_{w,i}}{\partial y} \right) \tag{1a}$$

and

$$\mathcal{B}^-(\Theta_{w,i}) := -k_w(0) \left. \frac{\partial \Theta_{w,i}}{\partial y} \right|_{y=0} - \dot{q}_{w,i} \tag{1b}$$

$$\mathcal{B}^+(\Theta_{w,i}) := \left. \Theta_{w,i} \right|_{y=d_w} - T_o, \tag{1c}$$

the heat conduction is determined by [2, 19]

$$\mathcal{D}\left(\Theta_{w,i}(y,t)\right) = 0 \qquad y \in [0, d_w]\,, t > t_0 \tag{1d}$$

with the boundary conditions

$$\mathcal{B}^-\left(\Theta_{w,i}(y,t)\right) = 0 \tag{1e}$$

$$\mathcal{B}^+\left(\Theta_{w,i}(y,t)\right) = 0 \tag{1f}$$

and the initial condition

$$\Theta_{w,i}(y, t_0) = \Theta_{w,i,0}(y) \qquad y \in [0, d_w]\,. \tag{1g}$$

T_o denotes the outer surface temperature of the wall and is assumed to be equal to the constant ambient temperature. Moreover, the heat flux density $\dot{q}_{w,i}$ defines the heat exchange between the wall and the furnace interior. Equation (1) is the so-called *strong formulation* of the heat conduction process.

2.1.2. Galerkin method for the heat conduction problem

For temperature-independent material parameters, i.e., $k_w(y, \Theta_{w,i}) = k_w(y)$ and $c_w(y, \Theta_{w,i}) = c_w(y)$, an approximate solution of Eq. (1) can be found by means of the Galerkin weighted residual method [4, 12, 13, 50]. Let $\mathcal{V}$ be a function space on the domain $[0, d_w]$ so that the functions $v \in \mathcal{V}$ ensure the finiteness of the integrals in the following relations. Equation (1) is satisfied if

$$0 = \int_0^{d_w} v(y) \mathcal{D}(\Theta_{w,i}(y,t)) \mathrm{d}y + v^- \mathcal{B}^-(\Theta_{w,i}(y,t)) + v^+ \mathcal{B}^+(\Theta_{w,i}(y,t)) \qquad t > t_0.$$

holds for arbitrary functions $v(y) \in \mathcal{V}$ and for arbitrary scalars $v^\pm \in \mathbb{R}$. As demonstrated in [49], choosing $v^+ = v(d_w)$ and $v^- = v(0)$ gives a useful simplification especially for Neumann boundary conditions and therefore, this choice is used throughout this analysis. Next, integration by parts yields the so-called

Post-print version of the article: M. Niederer, S. Strommer, A. Steinboeck, and A. Kugi, "A simple control-oriented model of an indirect-fired strip annealing furnace", *International Journal of Heat and Mass Transfer*, vol. 78, pp. 557–570, 2014. DOI: 10.1016/j.ijheatmasstransfer.2014.06.080

weak formulation of the heat conduction problem

$$0 = \int_0^{d_w} v(y)\rho_w(y)c_w(y)\frac{\partial\Theta_{w,i}(y,t)}{\partial t}\mathrm{d}y + \int_0^{d_w}\frac{\partial v(y)}{\partial y}k_w(y)\frac{\partial\Theta_{w,i}(y,t)}{\partial y}\mathrm{d}y - v(0)\dot{q}_{w,i} - v(d_w)k_w(d_w)\left.\frac{\partial\Theta_{w,i}(y,t)}{\partial y}\right|_{y=d_w} + v(d_w)\left(\Theta_{w,i}(d_w,t) - T_o\right). \tag{2}$$

Compared to Eq. (1d), Eq. (2) demands less restrictive requirements concerning the differentiability of $\Theta_{w,i}(y,t)$ with respect to y. Equation (2) is the basis for an approximate solution of the heat conduction problem by means of the Galerkin method. It uses the approximation

$$\hat{\Theta}_{w,i}(y,t) = h^0_{w,i}(y) + \sum_{r=1}^{N_G} h^r_{w,i}(y)T^r_{w,i}(t), \tag{3}$$

for the temperature field $\Theta_{w,i}(y,t)$. In Eq. (3), $h^0_{w,i}(y)$ is introduced to satisfy the homogeneous boundary conditions, $h^r_{w,i}(y) \in \mathcal{V}_h = \mathrm{span}\{h^1_{w,i}, h^2_{w,i}, \dots, h^{N_G}_{w,i}\} \subset \mathcal{V}$ are known analytic functions that are called *trial* functions, and $T^r_{w,i}(t)$ are the *Galerkin* coefficients. In general the approximation (3) does not fulfill Eq. (1d). However, Eq. (2) with $\Theta_{w,i}(y,t)$ replaced by $\hat{\Theta}_{w,i}(y,t)$ from Eq. (3) gives a reasonable approximation if the functions $h^r_{w,i}(y)$ are also used as trial function $v(y)$ in Eq. (2). Thus, evaluation of Eq. (2) by sequential replacement of $v(y)$ with the N_G trial functions $h^r_{w,i}(y)$ yields a system of ordinary differential equations for the unknown Galerkin coefficients $T^r_{w,i}(t)$. Because $\mathcal{D}(\hat{\Theta}_{w,i}(y,t))$ and $\mathcal{B}^{\pm}(\hat{\Theta}_{w,i}(y,t))$ represent *residuals* or *errors* which are weighted and integrated, the chosen approach is often called method of weighted residuals.

A reasonable choice for the approximation $\hat{\Theta}_{w,i}(y,t)$ from Eq. (3) can be found by using the steady-state solution of the heat conduction problem (1d) for a multi-layered furnace wall with temperature-independent material parameters. It is piecewise linear and is given by [19]

$$\Theta^{stat}_{w,i,j}(y,t) = \left(\Theta_{w,i}(0,t) - T_o\right)\underbrace{\frac{\sum_{l=j}^{J}\frac{d_{w,l}}{k_{w,l}} - \frac{y-y_{j-1}}{k_{w,j}}}{\sum_{l=1}^{J}\frac{d_{w,l}}{k_{w,l}}}}_{h_{w,i,j}(y)} + T_o, \quad y \in [y_{j-1}, y_j], \tag{4}$$

where $y_0 = 0$, $y_j = \sum_{l=1}^{j} d_{w,l}$, and $j = 1, \dots, J$. Thus, the Galerkin approach reads as

$$\hat{\Theta}_{w,i}(y,t) = \left(1 - h_{w,i}(y)\right)T_o + h_{w,i}(y)T_{w,i}(t) \tag{5}$$

with the trial function $v(y) = h_{w,i}(y)$ that assembles the functions $h_{w,i,j}(y)$ from Eq. (4) with $y \in [0, d_w]$ and the time-dependent Galerkin coefficient $T_{w,i}$. Since $h_{w,i}(d_w) = 0$, the approximation (5) satisfies the boundary condition at $y = d_w$. $T_{w,i}$ represents the inner surface temperature of the furnace wall, i.e., $T_{w,i} = \Theta_{w,i}(0,t)$, which is also required for the calculation of the radiative heat transfer inside the furnace.

The ordinary differential equation obtained from the Galerkin method takes the form

$$\frac{\mathrm{d}}{\mathrm{d}t}T_{w,i} = \frac{1}{K_1}\dot{q}_{w,i} - \frac{K_2}{K_1}\left(T_{w,i} - T_o\right), \tag{6a}$$

with the abbreviations

$$K_1 = \left(\sum_{j=1}^{J}\frac{d_{w,j}}{k_{w,j}}\right)^{-2}\sum_{j=1}^{J}\frac{\rho_{w,j}c_{w,j}k_{w,j}}{3}\left(\left(\sum_{l=j}^{J}\frac{d_{w,l}}{k_{w,l}}\right)^3 - \left(\sum_{l=j+1}^{J}\frac{d_{w,l}}{k_{w,l}}\right)^3\right) \tag{6b}$$

$$K_2 = \left(\sum_{j=1}^{J}\frac{d_{w,j}}{k_{w,j}}\right)^{-1}. \tag{6c}$$

For an approximate consideration of the temperature-dependence of the material parameters, the stationary solution $\Theta^{stat}_{w,i}(y,t)$ of the heat conduction problem (1) is used. It is assumed that the material parameters of the individual layers are determined by the average temperature of each layer, i.e., $k_{w,i,j}(\Theta^{stat}_{w,i}((y_{j-1}+y_j)/2,t))$ and $c_{w,i,j}(\Theta^{stat}_{w,i}((y_{j-1}+y_j)/2,t))$, $j = 1, \dots, J$. For a given surface temperature $\Theta_{w,i}(0,t)$, the temperatures $\Theta^{stat}_{w,i}((y_{j-1}+y_j)/2,t)$ can thus be calculated by solving the resulting (nonlinear) system of equations, cf. Eq. (4). Since $T_{w,i} = \Theta_{w,i}(0,t)$, the abbreviations K_1 and K_2 can be calculated as functions of the Galerkin coefficient $T_{w,i}$ by using the material parameters evaluated at the temperatures $\Theta^{stat}_{w,i}((y_{j-1}+y_j)/2,t)$, $j = 1, \dots, J$, i.e., $K_1(T_{w,i})$ and $K_2(T_{w,i})$. Note that with this approach the steady-state solution of Eq. (6) equals the steady-state solution of the heat conduction problem (1d).

For the real-time implementation, $K_1(T_{w,i})$ and $K_2(T_{w,i})$ are stored in advance for various values of $T_{w,i}$ and linear interpolation is employed. This facilitates a computationally undemanding evaluation of Eq.(6a).

The partition wall inside the furnace (cf. Fig. 1) has a slightly different structure compared to the outer furnace walls. It consists of several thin plates that are installed side-by-side with a thermal inertia that is negligibly small. For this reason, the partition wall is assumed to act just as a radiation shield between the two furnace sections RTH and RTS [2], i.e., two corresponding points on both surfaces of the wall have the same temperature. The accuracy of this assumption can be shown by consideration of the dynamic behavior of the wall and by using the singular perturbation method [23].

2.2. W-shaped radiant tube

As shown in Fig. 3, the main components of a W-shaped radiant tube are the burner, the tube, and the local recuperator for preheating the combustion air. The heat released by the combustion process inside the radiant tube is either transferred to the furnace chamber by thermal conduction in the wall of the radiant tube or it is lost in the form of sensible heat of the exhaust gas leaving the radiant tube after the recuperator. In order to obtain a tractable, low-dimensional model of a radiant tube, the combustion within the radiant tube and the thermal conduction through the tube wall are considered by simple balance

Post-print version of the article: M. Niederer, S. Strommer, A. Steinboeck, and A. Kugi, "A simple control-oriented model of an indirect-fired strip annealing furnace", *International Journal of Heat and Mass Transfer*, vol. 78, pp. 557–570, 2014. DOI: 10.1016/j.ijheatmasstransfer.2014.06.080

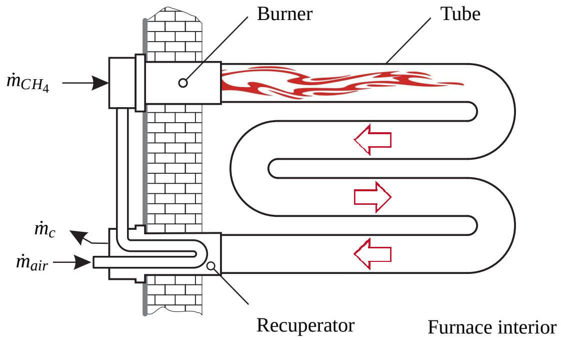

Figure 3: W-shaped radiant tube.

models.

2.2.1. *Assumptions*

The following assumptions may fail to capture the physical behavior of a radiant tube to a nicety. However, they yield a mathematical model that is low-dimensional and constitutes a good compromise between accuracy and computational efficiency.

- The combustion of natural gas inside the radiant tube is assumed to be complete and stationary. Hence, there is no natural gas left in the exhaust gas. This assumption is justified because the burners operate in a fuel-lean mode, i.e., with excess air ($\lambda > 1$).
- It is assumed that the combustion and the heat exchange from the flue gas to the radiant tube wall are independent of the temperature of the radiant tube wall. Since the combustion temperature is relatively high, this seems to be an acceptable assumption.
- It is assumed that a radiant tube consists of four straight pipes. That is, the bendings of the tube are neglected. Moreover, the heat flow through the wall of the radiant tube decreases from the first to the last pipe since the flue gas temperature decreases along the tube. Therefore, the combustion heat that is not lost with the exhaust gas is non-uniformly allocated to the four pipes. Furthermore, it is assumed that within each straight pipe the heat flux is uniformly distributed over the surface of the pipe.

2.2.2. *Combustion*

In the considered furnace, the burners are operated with natural gas, which is more or less pure methane (CH_4). The supply of combustion air depends on the mass flow of fuel and on the excess air coefficient [47]. In the currently used control strategy, the excess air coefficient is selected according a user-defined setpoint curve that is parameterized with the mass flow of fuel. The flue gas consists mainly of carbon dioxide, oxygen, water, and nitrogen and leaves the radiant tube after passing the recuperator. Abbreviations for the flue gas components are summarized in the set $\mathcal{S}_\nu = \{CO_2, O_2, H_2O, N_2\}$.

In the following, a single radiant tube i (including the recuperator) is considered as an input/output system. Its input quantities are the mass flow of fuel $\dot{m}_{CH_4}$ and the mass flows of oxygen $\dot{m}_{O_2}$ and nitrogen $\dot{m}_{N_2}$, i.e., the combustion air. Furthermore, the output quantities are the mass flow of exhaust gas $\dot{m}_c$ and the heat input $\dot{Q}_{c,i}$ that is transferred through the wall of the radiant tube i by means of thermal conduction.

Since the combustion inside the radiant tube is assumed to be complete, i.e., $\lambda > 1$, the corresponding stationary reaction equation reads as

$$\begin{aligned} CH_4 + 2\lambda\,(O_2 + 3.76N_2) \longrightarrow& \\ CO_2 + 2H_2O + 2(\lambda-1)O_2 + 7.52\lambda N_2&. \end{aligned} \tag{7}$$

Therefore, the incoming mass flows are coupled by

$$\dot{m}_\kappa = \zeta_\kappa(\lambda)\frac{M_\kappa}{M_{CH_4}}\dot{m}_{CH_4} \tag{8}$$

with $\kappa \in \mathcal{S}_\kappa = \{CH_4, O_2, N_2\}$ and $(\kappa, \zeta_\kappa) \in \{(CH_4, 1), (O_2, 2\lambda), (N_2, 7.52\lambda)\}$. Moreover, M_κ denotes the molar mass of the component κ. Based on Eq. (7), the outgoing mass flows are defined as

$$\dot{m}_{c,\nu} = \zeta_\nu(\lambda)\frac{M_\nu}{M_{CH_4}}\dot{m}_{CH_4} \tag{9}$$

with $\nu \in \mathcal{S}_\nu$ and $(\nu, \zeta_\nu) \in \{(CO_2, 1), (H_2O, 2), (O_2, 2(\lambda-1)), (N_2, 7.52\lambda)\}$. Finally, the heat input $\dot{Q}_{c,i}$ follows from the energy balance [31] in the form

$$\begin{aligned} \dot{Q}_{c,i} = \underbrace{\sum_{\kappa\in\mathcal{S}_\kappa}\frac{\dot{m}_\kappa}{M_\kappa}\Delta\bar{h}^0_\kappa - \sum_{\nu\in\mathcal{S}_\nu}\frac{\dot{m}_{c,\nu}}{M_\nu}\Delta\bar{h}^0_\nu}_{\text{Latent heat}} \\ + \underbrace{\sum_{\kappa\in\mathcal{S}_\kappa}\frac{\dot{m}_\kappa}{M_\kappa}\bar{h}_\kappa(T_\kappa) - \sum_{\nu\in\mathcal{S}_\nu}\frac{\dot{m}_{c,\nu}}{M_\nu}\bar{h}_\nu(T_c)}_{\text{Sensible heat}}, \end{aligned} \tag{10}$$

where $\bar{h}_j(T)$ and $\Delta\bar{h}^0_j$ with $j \in \mathcal{S}_\kappa \cup \mathcal{S}_\nu$ describe the specific enthalpy per mol and the enthalpy of reaction per mol, respectively. $\Delta\bar{h}^0_j$ can be calculated from tabulated values [24, 35]. T_κ with $\kappa \in \mathcal{S}_\kappa$ are the known temperatures of the fuel and the combustion air, respectively. Furthermore, T_c is the temperature of the exhaust gas that leaves the radiant tube after the recuperator.

In normal operation, the mass flows $\dot{m}_{CH_4}$, $\dot{m}_{O_2}$, $\dot{m}_{N_2}$, and thus $\dot{m}_c = \sum_{\nu\in\mathcal{S}_\nu}\dot{m}_{c,\nu} = \dot{m}_{CH_4} + \dot{m}_{O_2} + \dot{m}_{N_2}$ are known, cf. Eqs. (8) and (9). The excess air coefficient λ is determined by a user-defined set-point curve $\lambda(\dot{m}_{CH_4})$. The temperature T_c of the exhaust gas is only measured at a few points in each control zone. Based on these measurement values, the exhaust gas temperature of all other radiant tubes is estimated by linear interpolation. Hence, the heat input $\dot{Q}_{c,i}(\dot{m}_{CH_4}, T_c)$ that is transferred through the wall of an individual radiant tube can be computed by means of Eq. (10).

Since the mathematical model does not feature an analytical description of the exhaust gas temperature T_c, the heat input $\dot{Q}_{c,i}$ cannot be precisely determined without measurement. However, especially for control and optimization as well as for off-line studies, the calculation of $\dot{Q}_{c,i}$ independent of T_c is es-

Post-print version of the article: M. Niederer, S. Strommer, A. Steinboeck, and A. Kugi, "A simple control-oriented model of an indirect-fired strip annealing furnace", *International Journal of Heat and Mass Transfer*, vol. 78, pp. 557–570, 2014. DOI: 10.1016/j.ijheatmasstransfer.2014.06.080

sential. For this reason, an approximate static mapping between the mass flow of fuel and the heat input is derived. Let Δh_f^0 be the reaction enthalpy of one unit of fuel that is released by the combustion process, which is also known as calorific value. Using Eqs. (8) and (9) in the expression for the latent heat in Eq. (10), Δh_f^0 reads as

$$\Delta h_f^0 = \frac{\Delta \bar{h}^0_{CH_4} + \Delta \bar{h}^0_{O_2} - \Delta \bar{h}^0_{CO_2} - 2\Delta \bar{h}^0_{H_2O}}{M_{CH_4}}. \tag{11}$$

Thus, the reaction enthalpy $\dot{m}_{CH_4}\Delta h_f^0$ describes the primary energy that is released by an isothermal combustion of the fuel. If the measured values T_κ, T_c, and $\dot{m}_{CH_4}$ of an individual radiant tube are used as input parameters in Eqs. (10) and (11), the empirical relationship between the reaction enthalpy $\dot{m}_{CH_4}\Delta h_f^0$ and the heat input $\dot{Q}_{c,i}$ shown in Fig. 4 is obtained. $\dot{Q}_{c,i}$ depends significantly on λ because excess air that is heated from room temperature to T_c is a heat sink and increases the required primary energy. In the considered furnace, the radiant tubes are operated with a user-defined set-point curve $\lambda(\dot{m}_{CH_4})$ that does not change. Moreover, it is assumed that T_κ, $\forall\kappa \in \mathcal{S}_\kappa$, is constant and that there exists a unique continuous function $T_c(\dot{m}_{CH_4})$. Generally, T_c depends on $\dot{m}_{CH_4}$, λ, the flow conditions inside the radiant tube and the recuperator, and their temperature states. This implies that there is a weak influence of the furnace interior on T_c by the temperature state of the radiant tube wall. As analyzed in [33], this weak influence can be neglected without compromising the accuracy. Based on these stipulations, there exists a function (static mapping)

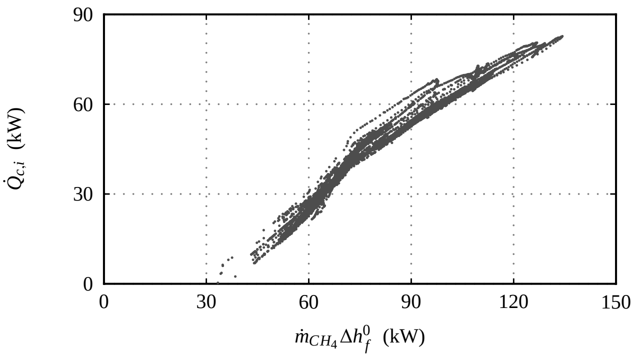

Figure 4: Relationship between the reaction enthalpy $\dot{m}_{CH_4}\Delta h_f^0$ and the heat input $\dot{Q}_{c,i}$.

$$\dot{Q}_{c,i} = \psi(\dot{m}_{CH_4}) \tag{12}$$

that can be obtained by smoothing the measured curve shown in Fig. 4 as a function of $\dot{m}_{CH_4}$. Note that the shape of $\psi(\dot{m}_{CH_4})$ is mainly determined by the underlying set-point curve $\lambda(\dot{m}_{CH_4})$.

2.2.3. Heat conduction through the wall of the radiant tube

Consider that the heat input $\dot{Q}_{c,i}(\dot{m}_{CH_4}, T_c)$ is (non-uniformly) distributed over the four pipes $j = 1, 2, 3, 4$ of a single W-shaped radiant tube i according to the weighting factors $g_j \geq 0$ with $\sum_{j=1}^4 g_j = 1$. In this paper, the weighting factors g_j are determined by means of a radiation balance and a measured characteristic temperature profile along the radiant tube [20]. Let D_r be the mean diameter and d_r the thickness of a pipe, as shown in Fig. 5. Since the dimension of the pipe is characterized by $D_r \gg d_r$, a Cartesian coordinate system is a reasonable assumption, i.e., the pipe bend is neglected. Furthermore, the mean area of each pipe j can be written in the form

$$S_r = L_r \pi D_r,$$

where L_r denotes the length of the pipe, which is assumed to equal the width of the furnace. Thus, the (local) heat flux at the surface of each pipe, as indicated in Fig. 5, reads as

$$\dot{q}_{c,i,j} = g_j \frac{\dot{Q}_{c,i}}{S_r}.$$

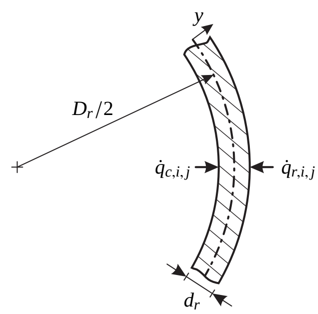

Figure 5: Section of the radiant tube wall.

Let $\Theta_{r,i,j}(y,t)$ be the temperature field in the wall of a pipe j defined along the direction $y \in [-d_r/2, d_r/2]$, as indicated in Fig. 5. For modeling the temperature evolution of the pipe, a 1-dimensional heat conduction is considered. By using the notation of differential operators (cf. Sec. 2.1.1), the heat conduction equation reads as

$$\mathcal{D}(\Theta_{r,i,j}(y,t)) := \rho_r c_r \frac{\partial \Theta_{r,i,j}(y,t)}{\partial t} - \frac{\partial}{\partial y}\left(k_r \frac{\partial \Theta_{r,i,j}(y,t)}{\partial y}\right) = 0 \tag{13a}$$

with the Neumann boundary conditions

$$\mathcal{B}^-(\Theta_{r,i,j}(y,t)) := -k_r \left.\frac{\partial \Theta_{r,i,j}(y,t)}{\partial y}\right|_{y=-d_r/2} - \dot{q}_{c,i,j} = 0 \tag{13b}$$

$$\mathcal{B}^+(\Theta_{r,i,j}(y,t)) := k_r \left.\frac{\partial \Theta_{r,i,j}(y,t)}{\partial y}\right|_{y=d_r/2} - \dot{q}_{r,i,j} = 0 \tag{13c}$$

and the initial condition

$$\Theta_{r,i,j}(y,t_0) = \Theta_{r,i,j,0}(y) \tag{13d}$$

for $y \in [-d_r/2, d_r/2]$ and $t > t_0$. Here, k_r, c_r, and ρ_r denote the thermal conductivity, the specific heat capacity, and the constant mass density, respectively. The parameters k_r and c_r are temperature-dependent. Moreover, $\dot{q}_{r,i,j}$ defines the heat flux

Post-print version of the article: M. Niederer, S. Strommer, A. Steinboeck, and A. Kugi, "A simple control-oriented model of an indirect-fired strip annealing furnace", *International Journal of Heat and Mass Transfer*, vol. 78, pp. 557–570, 2014. DOI: 10.1016/j.ijheatmasstransfer.2014.06.080

from the pipe j to the furnace interior.

Since the Biot number [2] is much smaller than unity, it is acceptable to assume a uniform temperature profile $\Theta_{r,i,j}(y,t)$ along the direction y, i.e., $\hat{\Theta}_{r,i,j}(y,t) = T_{r,i,j}(t)$. In terms of the Galerkin approach, $T_{r,i,j}$ is the time-dependent Galerkin coefficient and $h_{r,i,j}(y) = 1$ is the constant trial function. $T_{r,i,j}(t)$ also represents the mean temperature of the radiant tube wall. An approximate solution of the heat conduction problem (13) can be derived by using its weak formulation and insertion of the approximation $\hat{\Theta}_{r,i,j} = T_{r,i,j}(t)$ and $h_{r,i,j}(y) = 1$ as trial function. Thus, the heat conduction problem results in an ordinary differential equation for the Galerkin coefficient $T_{r,i,j}$, i.e.,

$$\frac{\mathrm{d}}{\mathrm{d}t} T_{r,i,j} = \frac{1}{\rho_r c_r(T_{r,i,j}) d_r} \left(\dot{q}_{r,i,j} + \dot{q}_{c,i,j} \right). \tag{14}$$

Equation (14) equals a simple heat balance for the tube wall. Finally, by introducing the vectors $\mathbf{T}_{r,i} = \left[T_{r,i,j}\right]_{j=1,\ldots,4}$, $\dot{\mathbf{q}}_{r,i} = \left[\dot{q}_{r,i,j}\right]_{j=1,\ldots,4}$, $\dot{\mathbf{q}}_{c,i} = \left[\dot{q}_{c,i,j}\right]_{j=1,\ldots,4} = \left[g_j \dot{Q}_{c,i}/S_r\right]_{j=1,\ldots,4}$, and $\mathbf{c}_r(\mathbf{T}_{r,i}) = \left[c_r(T_{r,i,j})\right]_{j=1,\ldots,4}$, the complete model of a W-shaped radiant tube can be written in the form

$$\frac{\mathrm{d}}{\mathrm{d}t} \mathbf{T}_{r,i} = \mathrm{diag}\{\rho_r d_r \mathbf{c}_r(\mathbf{T}_{r,i})\}^{-1} \left(\dot{\mathbf{q}}_{c,i} + \dot{\mathbf{q}}_{r,i} \right), \tag{15}$$

where $\mathrm{diag}\{\rho_r d_r \mathbf{c}_r(\mathbf{T}_{r,i})\}$ denotes a diagonal matrix with $\rho_r d_r c_r(T_{r,i,j})$, $j = 1, \ldots, 4$, as diagonal elements.

2.3. Strip

This section addresses the heat balance of the strip. As mentioned in Sec. 1.4, most published furnace models use Eulerian coordinates for describing the strip motion. However, in this analysis, Lagrangian coordinates are used, because they allow a precise representation of the temperature profile along the strip, in particular when a welded joint that connects two different strips passes through the furnace.

2.3.1. Energy balance

The processed strip is characterized by its geometry and material parameters. Let d_s be the thickness and b_s the width of the strip, which is assumed to move always in the center of the furnace. The material parameters of the strip, i.e., the specific heat capacity c_s, the mass density ρ_s, and the thermal conductivity k_s, usually depend on the strip temperature $T_{\tilde{s}}$ and may vary from strip to strip. Consider that the strip moves with the velocity v_s along the direction z as indicated in Fig. 6. The value v_s may vary during the furnace operation depending on the product and possible operational requirements of up- or down-stream process steps. As mentioned, Lagrangian coordinates are used to describe the strip motion. The (local) Lagrangian coordinate $\tilde{z}$ is fixed to a given material point whereas the Eulerian coordinate z is spatially fixed. The mapping between Lagrangian and Eulerian coordinates is thus given by

$$z = \tilde{z} + \int_{t_0}^{t} v_s(\tau) \mathrm{d}\tau,$$

which implies $z = \tilde{z}$ for $t = t_0$.

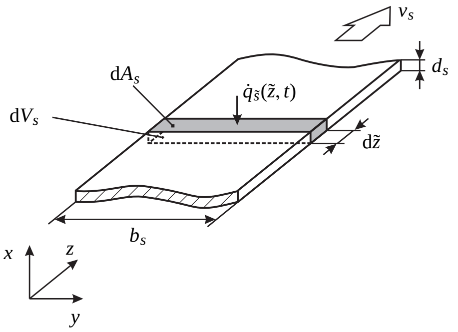

Figure 6: Moving strip.

In consideration of the Biot number [2] that is much smaller than unity, the strip temperature $T_{\tilde{s}}$ along the direction x is assumed homogeneous. Moreover, the heat conduction along the strip is neglected because the diffusive heat transport is generally significant lower than the convective heat transport due to the motion of the strip. For this reason, a heat balance of an infinitesimal volume element $\mathrm{d}V_s$ is considered to model the temperature profile of the strip by means of ordinary differential equations. Let $\dot{q}_{\tilde{s}}$ be the (total) heat flux into the surface $\mathrm{d}A_s$ of the considered volume element as indicated in Fig. 6. Two types of heat exchange are relevant for the strip: a) heat transfer between the strip and the deflection rolls by conduction, which is addressed in Sec. 2.4, and b) heat transfer by radiation, which is analyzed in Sec. 2.5. The heat transfer by convection is neglected since the temperature in the furnace chamber is relatively high and, therefore, thermal radiation is the dominant mode of heat transfer [5, 14, 45]. Thus, the heat balance in Lagrangian coordinates [2, 19] reads as

$$\frac{\mathrm{d}}{\mathrm{d}t} T_{\tilde{s}}(\tilde{z},t) = \frac{2\dot{q}_{\tilde{s}}(\tilde{z},t)}{\rho_s c_s(T_{\tilde{s}}(\tilde{z},t)) d_s}, \tag{16}$$

with the mass density ρ_s, the temperature-dependent specific heat capacity c_s, the strip thickness d_s and the initial condition $T_{\tilde{s}}(\tilde{z},t_0) = T_{\tilde{s},0}(\tilde{z})$.

2.3.2. Mapping between the Lagrangian and Eulerian framework

The analysis of the radiative heat transfer requires the strip temperatures in Eulerian coordinates. Since the strip is described in Lagrangian coordinates, a simple mapping scheme is indicated in Fig. 7. Consider that $T_{\tilde{s},i}$ are the strip temperatures at the nodal points (Lagrangian coordinates) $\tilde{z}_i$, $i = 1, \ldots, N_{\tilde{s}}$, i.e., $T_{\tilde{s},i} = T_{\tilde{s}}(\tilde{z}_i, t)$. Moreover, they are assumed to be homogeneous in the corresponding strip section $[\tilde{z}_i, \tilde{z}_{i-1})$. For the radiative heat transfer analysis, the temperature $T_{s,j} = T_s(z_j, t)$ of the strip surface S_j in the range $z \in \left[z_j, z_{j+1}\right)$ in the Eulerian reference system is of interest. The temperature is assumed to be homogeneous within the range $\left[z_j, z_{j+1}\right)$ and can be approx-

Post-print version of the article: M. Niederer, S. Strommer, A. Steinboeck, and A. Kugi, "A simple control-oriented model of an indirect-fired strip annealing furnace", *International Journal of Heat and Mass Transfer*, vol. 78, pp. 557–570, 2014. DOI: 10.1016/j.ijheatmasstransfer.2014.06.080
The content of this post-print version is identical to the published paper but without the publisher's final layout or copy editing.

imately computed by means of

$$T_{s,j} = \frac{1}{z_{j+1} - z_j} \int_{z_j}^{z_{j+1}} T_{\tilde{s}}(\underbrace{z - \int_{t_0}^{t} v_s(\tau)\mathrm{d}\tau}_{=\tilde{z}}, t)\mathrm{d}z, \quad \forall j = 1, \ldots, N_s \tag{17}$$

where N_s is the number of discrete strip sections in Eulerian coordinates. In matrix notation, Eq. (17) reads as $\mathbf{T}_s = \mathbf{M}_T \mathbf{T}_{\tilde{s}}$ with $\mathbf{T}_s = \left[T_{s,j}\right]_{j=1,\ldots,N_s}$, $\mathbf{T}_{\tilde{s}} = [T_{\tilde{s},i}]_{i=1,\ldots,N_{\tilde{s}}}$, and the mapping matrix $\mathbf{M}_T \in \mathbb{R}^{N_s \times N_{\tilde{s}}}$. The mean temperatures $\mathbf{T}_s$ are subsequently used for calculating the radiative heat exchange as described in Sec. 2.5.

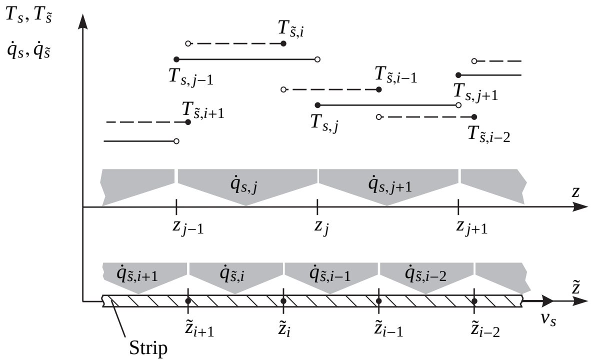

Figure 7: Mapping of temperatures and heat fluxes between Eulerian and Lagrangian coordinates.

The net radiation method, which is used for the calculation of the radiative heat transfer in the furnace, yields the local heat fluxes $\dot{q}_{s,j}$ into the spatially fixed strip sections $j = 1, \ldots, N_s$ defined in the Eulerian reference system. It suggests that the heat fluxes $\dot{q}_{s,j} = \dot{q}_s(z)|_{z\in[z_{j-1},z_j)}$ into the strip sections are piecewise constant along the strip. Equation (16) is evaluated at the points $\tilde{z}_i$, $i = 1, \ldots, N_{\tilde{s}}$ in the Lagrangian reference system. Hence, the heat flux $\dot{q}_{\tilde{s}}$ is required at these points and the heat flux values computed in the Eulerian reference system have to be transformed back to the Lagrangian coordinate frame. This is done by means of

$$\dot{q}_{\tilde{s},i} = \frac{1}{\tilde{z}_{i+1} - \tilde{z}_i} \int_{\tilde{z}_i}^{\tilde{z}_{i+1}} \dot{q}_s(\underbrace{\tilde{z} + \int_{t_0}^{t} v(\tau)\mathrm{d}\tau}_{=z}, t)\mathrm{d}\tilde{z}, \quad \forall i = 1, \ldots N_{\tilde{s}},$$

which can be written in the form $\dot{\mathbf{q}}_{\tilde{s}} = \mathbf{M}_q \dot{\mathbf{q}}_s$ with $\dot{\mathbf{q}}_{\tilde{s}} = [\dot{q}_{\tilde{s},i}]_{i=1,\ldots,N_{\tilde{s}}}$, $\dot{\mathbf{q}}_s = \left[\dot{q}_{s,j}\right]_{j=1,\ldots,N_s}$, and the mapping matrix $\mathbf{M}_q \in \mathbb{R}^{N_{\tilde{s}} \times N_s}$.

2.4. Deflection roll

The processed strip is conveyed through the furnace by means of N_d deflection rolls, cf. Fig. 1. There is heat exchange between the rolls and the strip by means of heat conduction. Since the thermal inertia of the rolls cannot be neglected in terms of the dynamic behavior of the strip temperature, they are modeled as lumped parameter systems with a homogeneous temperature.

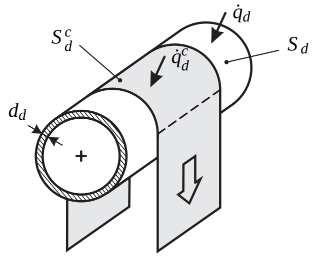

Figure 8: Deflection roll.

An individual deflection roll i is constructed as a hollow cylinder with the surface area S_d and the wall thickness d_d as shown in Fig. 8. Moreover, let $S_{d,i}^c < S_d$ be the contact area between the strip and the roll. To model the evolution of the (homogeneous) roll temperature $T_{d,i}$, a simple heat balance is used. This results in

$$\frac{\mathrm{d}}{\mathrm{d}t} T_{d,i} = \frac{1}{\rho_d c_d(T_{d,i}) d_d} \left(\left(1 - \frac{S_{d,i}^c}{S_d}\right) \dot{q}_{d,i} + \frac{S_{d,i}^c}{S_d} \dot{q}_{d,i}^c \right), \tag{18}$$

with the heat capacity $c_d(T_{d,i})$ and the mass density ρ_d. The heat fluxes $\dot{q}_{d,i}$ and $\dot{q}_{d,i}^c$ are determined by the heat transfer mechanisms radiation with the furnace interior (cf. Sec. 2.5) and conduction with the strip, respectively. If T_s denotes the local temperature of the strip that is in contact with the deflection roll, the conductive heat flux into the respective roll reads as

$$\dot{q}_{d,i}^c = \frac{T_s - T_{d,i}}{R_c}, \tag{19}$$

with the thermal contact resistance R_c. Values of R_c are tabulated for various steel grades and contact pressures, cf. [19]. In a compact notation, Eq. (19) results in $\dot{\mathbf{q}}_d^c = 1/R_c \left(\mathbf{\Gamma}_T \mathbf{T}_s - \mathbf{T}_d\right)$ with $\dot{\mathbf{q}}_d^c = \left[\dot{q}_{d,i}^c\right]_{i=1,\ldots,N_d}$, $\mathbf{T}_d = [T_{d,i}]_{i=1,\ldots,N_d}$, and a sparse mapping matrix $\mathbf{\Gamma}_T \in \mathbb{R}^{N_d \times N_s}$ which selects the associated entries from the strip temperature vector $\mathbf{T}_s$ in the Eulerian reference system. Furthermore, the heat flux into the strip element that is in contact with the deflection roll is $-\dot{q}_{d,i}^c$. Thus, $-\mathbf{\Gamma}_q \dot{\mathbf{q}}_d^c$ with the sparse mapping matrix $\mathbf{\Gamma}_q \in \mathbb{R}^{N_s \times N_d}$, where $\mathbf{\Gamma}_T \mathbf{\Gamma}_q = \mathbf{E}$, gives the vector of heat fluxes into the strip in the Eulerian reference system.

2.5. Radiative heat transfer

The local heat fluxes into the surfaces in the furnace interior, i.e., the wall, the radiant tubes, the strip, and the deflection roll, are mainly caused by radiative heat transfer. Generally, radiative heat transfer induces heat exchange between all participating surfaces and is therefore a global phenomenon. To model the radiative heat transfer in the furnace, the *net-radiation-method* [16] is employed, where a multi-surface enclosure filled with non-participating gas is considered.

2.5.1. Assumptions

The most basic assumptions about radiation inside the furnace are listed in the following. These assumptions may neglect some of the peculiarities of radiative heat transfer in the

Post-print version of the article: M. Niederer, S. Strommer, A. Steinboeck, and A. Kugi, "A simple control-oriented model of an indirect-fired strip annealing furnace", *International Journal of Heat and Mass Transfer*, vol. 78, pp. 557–570, 2014. DOI: 10.1016/j.ijheatmasstransfer.2014.06.080

furnace. However, they yield a mathematical model that is suitable for an efficient calculation of the radiative heat flows.

- The temperature distribution of each participating surface is uniform. This assumption seems to be adequate for the deflection roll and a single pipe of a W-shaped radiant tube. For the strip and the furnace wall, the assumption is tenable if the chosen surface sections are sufficiently small.
- All participating surfaces behave like gray bodies. For the temperature range characterizing the normal operation of an indirect-fired furnace, this assumption seems to be acceptable.
- All participating surfaces are opaque and ideal diffuse reflectors, which means that the reflected fraction of the radiation energy that is incident on the surface does not depend on the direction of incidence.
- The inert gas, which flows through the furnace to protect the processed strip from oxidation, is assumed to be non-participating. Since inert gas is usually composed of diatomic molecules like N_2 and H_2, this is a reasonable postulate [21].

Remark: The influence of convection, especially forced convection for the moving strip, is neglected due to the high surface temperatures inside the furnace. To show the tenability of this assumption, the ratio

$$\frac{|\dot{q}_s^{conv}|}{|\dot{q}_s|} = \frac{|\alpha(v_s, T_{HNx})\,(T_{HNx} - T_s)\,|}{|\sigma\frac{\varepsilon_s\varepsilon_r}{\varepsilon_r+\varepsilon_s-\varepsilon_s\varepsilon_r}\left(\bar{T}_r^4 - T_s^4\right)|}$$

of the heat flux densities due to convection $\dot{q}_s^{conv}$ and radiation $\dot{q}_s$ is considered for an idealized furnace section.Here, T_{HNx} is the temperature of the inert gas, $\bar{T}_r$ is a mean temperature of the radiant tubes, T_s is the temperature of the strip and v_s the velocity of the strip. The average heat transfer coefficient $\alpha(v_s, T_{HNx})$ can be estimated by means of a flat plate [19] and a parallel flow and by using dimensionless numbers. For this estimation, the length of the strip between two deflection rolls is used as (characteristic) length of the plate. The magnitude of effect of the radiative heat transfer is estimated by considering two infinitely extended parallel surfaces with the temperatures $\bar{T}_r$ and T_s and the emissivities ε_r and ε_s. Moreover, σ denotes the Stefan-Boltzmann constant.

For this analysis, an average temperature $\bar{T}_r = 1250$ K of the radiant tubes is assumed. Furthermore, it is known from measurements that the temperature of the inert gas always exceeds 700 K, i.e., $T_{HNx} \in [700, 1250]$ K, and that the processed strip enters the indirect-fired furnace with approximately 850 K and leaves the furnace with a maximum temperature of 1200 K, i.e., $T_s \in [850, 1200]$ K. The strip velocity is in the range $v_s \in [1, 3]$ m/s. Since the heat transfer coefficient increases for higher strip velocities, the ratio $|\dot{q}_s^{conv}|/|\dot{q}_s|$ is evaluated for $v_s = 3$ m/s. Figure 9 shows that the effect of forced convection is only minor and that the neglect of this heat transfer mechanism is thus justified.

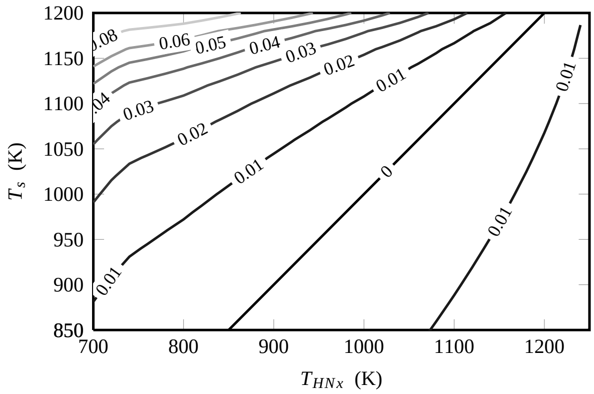

Figure 9: Contour plot of the ratio $|\dot{q}_s^{conv}|/|\dot{q}_s|$ of the heat flux densities due to convection and radiation.

2.5.2. Radiative heat transfer in a multi-surface enclosure

Consider a multi-surface enclosure of N discrete surface zones as shown in Fig. 10. The objective is to analyze the radiation exchange between these N surfaces, given that the surface temperatures, the surface areas, and the emissivities are known. A convenient means of analyzing this problem is the *net radiation method*, which was first devised by Hottel [16]. It should be mentioned that the net radiation method is a specialization of the *zone method* which also takes into account participating gaseous media between the surface zones [17, 18, 30, 41].

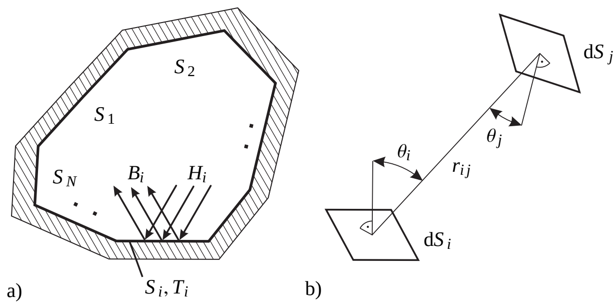

Figure 10: a) Multi-surface enclosure, b) Geometric relation between two infinitesimal surface sections.

For setting up the radiative energy balance of a discrete surface section, consider the i-th surface of the enclosure shown in Fig. 10 a). Here, the so-called *irradiance* H_i is the incident radiative energy per unit area of the surface S_i. Moreover, the emitted power of this surface is $\varepsilon_i\sigma T_i^4$. For $\varepsilon_i = 1$ (black body), the well known Stefan-Boltzmann law is obtained. The radiation emitted and reflected by the surface S_i can be combined to the *radiosity* B_i in the form

$$B_i = \varepsilon_i\sigma T_i^4 + (1 - \varepsilon_i)H_i. \tag{20}$$

The factor $1 - \varepsilon_i$ is due to *Kirchhoff's* law of thermal radiation [2, 15, 41] and is called *reflectivity*. Therefore, the net heat flux into the surface is defined by

$$\dot{q}_i = H_i - B_i. \tag{21}$$

Post-print version of the article: M. Niederer, S. Strommer, A. Steinboeck, and A. Kugi, "A simple control-oriented model of an indirect-fired strip annealing furnace", *International Journal of Heat and Mass Transfer*, vol. 78, pp. 557–570, 2014. DOI: 10.1016/j.ijheatmasstransfer.2014.06.080
The content of this post-print version is identical to the published paper but without the publisher's final layout or copy editing.

To describe the exchange of radiative energy within the enclosure, the geometry of the involved N surfaces has to be taken into account [2, 18, 30, 41]. Therefore, consider the two surfaces S_i and S_j, which are part of the enclosure. Let $S_i B_i$ be the total radiative power leaving the surface S_i. The portion of $S_i B_i$ that strikes the surface S_j is given by $\overline{s_i s_j} B_i$, where

$$\overline{s_i s_j} = \int_{S_i} \int_{S_j} \frac{\cos(\theta_i)\cos(\theta_j)}{\pi r_{ij}^2} \mathrm{d}S_j \mathrm{d}S_i \tag{22}$$

is called the *direct exchange area* [41, 30]. As indicated in Fig. 10 b), r_{ij} is the distance between two infinitesimal sections on the interacting surfaces S_i and S_j. Moreover, θ_i and θ_j denote the angles of incidence. Note that $\overline{s_i s_j}$ represents a purely geometric relation between the surfaces. Due to the symmetric occurrence of i and j in Eq. (22), the *reciprocity rule*

$$\overline{s_i s_j} = \overline{s_j s_i}$$

is obtained. Note that $\overline{s_i s_j}/S_i$ is the so-called *configuration factor* [2, 41].

In the next step, the balance of radiation energy in the multi-surface enclosure is derived. For that purpose, some matrices and vectors are introduced:

$$\begin{aligned}
&\overline{\mathbf{ss}} = \overline{\mathbf{ss}}^{\mathrm{T}} = \left[\overline{s_i s_j}\right]_{i=1,\dots,N, j=1,\dots,N}, \quad \boldsymbol{\varepsilon} = [\varepsilon_1, \varepsilon_2, \dots, \varepsilon_N]^{\mathrm{T}},\\
&\mathbf{H} = [H_1, H_2, \dots, H_N]^{\mathrm{T}}, \quad \mathbf{B} = [B_1, B_2, \dots, B_N]^{\mathrm{T}},\\
&\mathbf{S} = [S_1, S_2, \dots, S_N]^{\mathrm{T}}, \quad \dot{\mathbf{q}} = [\dot{q}_1, \dot{q}_2, \dots, \dot{q}_N]^{\mathrm{T}},\\
&\mathbf{T} = [T_1, T_2, \dots, T_N]^{\mathrm{T}}.
\end{aligned}$$

Summing up all incident fractions $\overline{s_i s_j} B_i$ for each surface section yields

$$\mathrm{diag}\{\mathbf{S}\}\mathbf{H} = \overline{\mathbf{ss}}\mathbf{B}. \tag{23}$$

Moreover, the counterparts of Eqs. (20) and (21) in matrix notation read as

$$\mathbf{B} = \mathrm{diag}\{\boldsymbol{\varepsilon}\}\sigma\mathbf{T}^4 + (\mathbf{I} - \mathrm{diag}\{\boldsymbol{\varepsilon}\})\mathbf{H} \tag{24a}$$

$$\dot{\mathbf{q}} = \mathbf{H} - \mathbf{B}. \tag{24b}$$

The 4$^{\text{th}}$ power in (24a) is applied to each component of the respective vector. Elimination of $\mathbf{B}$ and $\mathbf{H}$ in (23) and (24) yields the vector

$$\dot{\mathbf{q}} = \mathbf{P}\mathbf{T}^4 \tag{25}$$

of net heat fluxes into the surface zones with the abbreviation

$$\mathbf{P} = \sigma\mathrm{diag}\{\boldsymbol{\varepsilon}\}\left(\mathrm{diag}\{\mathbf{S}\} - \overline{\mathbf{ss}}(\mathbf{I} - \mathrm{diag}\{\boldsymbol{\varepsilon}\})\right)^{-1}\overline{\mathbf{ss}}\mathrm{diag}\{\boldsymbol{\varepsilon}\} - \sigma\mathrm{diag}\{\boldsymbol{\varepsilon}\}. \tag{26}$$

The matrix $\mathbf{P}$ depends only on the emissivities $\boldsymbol{\varepsilon}$ and the geometry of the enclosure. Therefore, Eq. (26) can be calculated in advance without any knowledge of the surface temperatures $\mathbf{T}$. For the real-time implementation, a computationally undemanding evaluation of Eq. (25) suffices to calculate the heat fluxes $\dot{\mathbf{q}}$.

Conservation of energy yields some algebraic constraints that are useful for calculating the exchange areas. These constraints are also known as *summation rules*. For their derivation, let the enclosure be in a state of thermal equilibrium. For this, all surface temperatures are equal and the net heat flows into the surface zones are zero, i.e., $\dot{\mathbf{q}} = \mathbf{0}$. The specialization of Eq. (24) for this state shows that $\mathbf{B} = \mathbf{H} = \sigma T^4 \mathbf{1}$ with the common temperature T. Here, $\mathbf{1}$ represents a vector with unity components only. Next, insertion into Eq. (23) yields the summation rule

$$\mathbf{S} = \overline{\mathbf{ss}}\mathbf{1}.$$

Moreover, the specialization of Eq. (25) for the state of thermal equilibrium yields

$$\mathbf{0} = \mathbf{P}\mathbf{1}.$$

2.5.3. Results for the furnace

The results of the previous section are now utilized for computing the net heat fluxes within the whole furnace. The most intricate part of this computation is to determine the direct exchange area matrix $\overline{\mathbf{ss}}$, cf. Eq. (22). In addition to the sophisticated 3-dimensional geometry, this computation is complicated by the fact that the strip width b_s changes during furnace operation. For this paper, the direct-exchange areas $\overline{\mathbf{ss}}$ for the full 3-dimensional geometry of the considered furnace was numerically calculated for a number of representative strip widths b_s by means of the software ANSYS. The resulting matrix $\mathbf{P} = \mathbf{P}(b_s)$ was then stored in a look-up table for these values b_s. If $\mathbf{P}(b_s)$ is required for some other strip widths, linear interpolation of the stored values may be used.

The net radiation method requires the participating surfaces to be discretized and the temperature and the emissivity have to be specified for each surface zone. For the strip, these quantities are only known in the Lagrangian reference frame. For this reason, the desired temperatures must be transformed to Eulerian coordinates using Eq. (17). Next, some vectors that summarize the temperatures of all participating surfaces are introduced:

$$\begin{aligned}
&\mathbf{T}_r = \left[\mathbf{T}_{r,1}^{\mathrm{T}}, \dots, \mathbf{T}_{r,N_r}^{\mathrm{T}}\right]^{\mathrm{T}}, \quad \mathbf{T}_w = [T_{w,1}, \dots, T_{w,N_w}]^{\mathrm{T}},\\
&\mathbf{T}_d = [T_{d,1}, \dots, T_{d,N_d}]^{\mathrm{T}}, \quad \mathbf{T}_s = [T_{s,1}, \dots, T_{s,N_s}]^{\mathrm{T}}.
\end{aligned}$$

Here, the indices $i \in \mathcal{I} = \{r, w, d, s\}$ refer to the radiant tubes, the furnace wall, the deflection rolls, and the strip, respectively. By analogy, the areas and the emissivities of the respective surface zones are summarized in the vectors $\mathbf{S}_i$ and $\boldsymbol{\varepsilon}_i$ with $i \in \mathcal{I}$, respectively. Furthermore, $\dot{\mathbf{q}}_i$ with $i \in \mathcal{I}$ are the net heat fluxes into the surfaces $\mathbf{S}_i$.

Finally, the heat exchange by radiation inside the entire indirect-fired furnace reads as, see also Eq. (25),

$$\begin{bmatrix} \dot{\mathbf{q}}_r \\ \dot{\mathbf{q}}_w \\ \dot{\mathbf{q}}_d \\ \dot{\mathbf{q}}_s \end{bmatrix} = \mathbf{P}(b_s) \begin{bmatrix} \mathbf{T}_r \\ \mathbf{T}_w \\ \mathbf{T}_d \\ \mathbf{T}_s \end{bmatrix}^4. \tag{27}$$

Post-print version of the article: M. Niederer, S. Strommer, A. Steinboeck, and A. Kugi, "A simple control-oriented model of an indirect-fired strip annealing furnace", *International Journal of Heat and Mass Transfer*, vol. 78, pp. 557–570, 2014. doi: 10.1016/j.ijheatmasstransfer.2014.06.080

2.6. Assembled system

In this section, the building blocks of the mathematical model of the indirect-fired furnace are assembled to obtain a complete dynamic simulation model of the furnace.

2.6.1. Continuous-time state space system

Using the heat transfer relations (19) and (27), the ordinary differential equations (6), (15), (16), and (18) can be written in the form

$$\frac{\mathrm{d}}{\mathrm{d}t}\begin{bmatrix}\mathbf{T}_r\\ \mathbf{T}_w\\ \mathbf{T}_d\\ \mathbf{T}_{\tilde{s}}\end{bmatrix} = \begin{bmatrix}\mathbf{f}_r(\mathbf{T}_r, \mathbf{T}_w, \mathbf{T}_d, \mathbf{T}_{\tilde{s}}, \mathbf{u}_m, \mathbf{u}_g, u_{\tilde{s}})\\ \mathbf{f}_w(\mathbf{T}_r, \mathbf{T}_w, \mathbf{T}_d, \mathbf{T}_{\tilde{s}}, u_{\tilde{s}})\\ \mathbf{f}_d(\mathbf{T}_r, \mathbf{T}_w, \mathbf{T}_d, \mathbf{T}_{\tilde{s}}, u_{\tilde{s}})\\ \mathbf{f}_{\tilde{s}}(t, \mathbf{T}_r, \mathbf{T}_w, \mathbf{T}_d, \mathbf{T}_{\tilde{s}}, u_{\tilde{s}})\end{bmatrix}. \tag{28}$$

The vector $\mathbf{T}_{\tilde{s}} = [\ldots, T_{\tilde{s},i}, T_{\tilde{s},i+1}, \ldots]$ summarizes the temperatures of the strip sections that are currently in the furnace. Since the strip is described in Lagrangian coordinates, the dimension of $\mathbf{T}_{\tilde{s}}$ varies and, therefore, Eq. (28) is a switched system. On the right-hand side of Eq. (28), $\mathbf{f}_w$ corresponds to Eq. (6), $\mathbf{f}_r$ to Eq. (15), $\mathbf{f}_d$ to Eq. (18), and $\mathbf{f}_{\tilde{s}}$ to Eq. (16). The explicit time-dependence of $\mathbf{f}_{\tilde{s}}$ refers to the different processed strips. Furthermore, the system inputs are the mass flow $\dot{m}_{CH4}$ of fuel to the N_z control zones, the (measured) exhaust gas temperatures T_c after the recuperator of each radiant tube as well as the strip temperature at the entry of the furnace (air lock). With $\dot{m}_{CH_4}$ and T_c, the heat input into the furnace chamber can be determined according to Eq. (10). If T_c is not available, i.e., in optimization or in off-line studies, the heat input can be approximated by means of Eq. (12). Let n_i be the number of all radiant tubes in a control zone i, i.e., $\sum_{i=1}^{N_z} n_i = N_r$ must hold. As all radiant tubes of a single control zone are uniformly supplied with fuel, the control input $\mathbf{u}_m$ reads as $\mathbf{u}_m = \left[\mathbf{u}_{m,1}^{\mathrm{T}}, \ldots, \mathbf{u}_{m,N_z}^{\mathrm{T}}\right]^{\mathrm{T}}$ with $\mathbf{u}_{m,i} = \mathbf{1}\dot{m}_{CH_4}^{i}/n_i \in \mathbb{R}^{n_i}$, $i = 1, \ldots, N_z$. Moreover, the exhaust gas temperatures can be combined into $\mathbf{u}_g = \left[\mathbf{u}_{g,1}^{\mathrm{T}}, \ldots, \mathbf{u}_{g,N_z}^{\mathrm{T}}\right]^{\mathrm{T}}$ with $\mathbf{u}_{g,i} = [T_{c,1}, \ldots, T_{c,n_i}]^{\mathrm{T}}$, $i = 1, \ldots, N_z$. The input $u_{\tilde{s}}$ is the temperature of the strip section that currently enters the furnace.

The interaction of the dynamical submodels describing the wall, the radiant tubes, the strip, and the deflection rolls caused by the heat transfer mechanisms radiation and conduction is outlined in Fig. 11. The inputs of these submodels are the heat fluxes $\dot{\mathbf{q}}_w$, $\dot{\mathbf{q}}_c + \dot{\mathbf{q}}_r$, $\dot{\mathbf{q}}_{\tilde{s}} = \mathbf{M}_q(\mathrm{diag}\{\mathbf{w}\}\dot{\mathbf{q}}_s - 1/2\mathbf{\Gamma}_q\dot{\mathbf{q}}_d^c)$, and $\dot{\mathbf{q}}_d$ and $\dot{\mathbf{q}}_d^c$, respectively. As suggested in Sec. 2.2.3, $\dot{\mathbf{q}}_c = [\dot{\mathbf{q}}_{c,i}]_{i=1,\ldots,N_r}$ denotes the heat fluxes on the inner surfaces of the radiant tube walls. Moreover, $\mathbf{w} \in \mathbb{R}^{N_s}$ is a vector with components $w_i \in \{\frac{1}{2}, 1\}$, where $i = 1, \ldots, N_s$. As for the second term of $\dot{\mathbf{q}}_{\tilde{s}}$, the value $\frac{1}{2}$ refers to strip sections that are in contact with deflection rolls. The most significant nonlinearity in Eq. (28) is the 4th-power stemming from the radiative heat transfer. Further nonlinearities are due to the material parameters, e.g., the specific heat capacity of the strip or the specific enthalpy per mol of the components of the exhaust gas.

2.6.2. Time discretization

The state space system (28) is defined in the continuous-time domain. However, for implementing the model on a computer system, the time domain has to be discretized. For this purpose, let $t_k, \forall k \in \mathbb{N}$, be the sampling points of the discretized time domain, which do not need to be equidistant. The corresponding sampling period is $\Delta t_k = t_{k+1} - t_k$. Since the continuous-time system does not allow an analytical solution of Eq. (28), its discrete-time representation can for instance be obtained by applying Euler's explicit method. Further possibilities to obtain a discrete-time representation of Eq. (28) are multi-stage Runge-Kutta methods, e.g., the *Heun* method or the *classical* Runge-Kutta method. Euler's explicit method is a 1-stage method of first order and is the simplest one-step method from the family of explicit Runge-Kutta methods. Generally, multi-stage Runge-Kutta methods are of higher accuracy order and compared to Euler's explicit method their stability region is larger. However, multi-stage methods require the repeated evaluation of the right-hand side of Eq. (28) and therefore significantly increase the computational costs. In view of the envisaged real-time implementation of the model, Euler's explicit method is used. Thus, the discrete-time model is given by

$$\mathbf{T}_{k+1} = \mathbf{T}_k + \Delta t_k \mathbf{f}_k(\mathbf{T}_k, \mathbf{u}_k) \tag{29}$$

with $\mathbf{T} = \left[\mathbf{T}_r^{\mathrm{T}}, \mathbf{T}_w^{\mathrm{T}}, \mathbf{T}_d^{\mathrm{T}}, \mathbf{T}_{\tilde{s}}^{\mathrm{T}}\right]^{\mathrm{T}}$, $\mathbf{u} = \left[\mathbf{u}_m^{\mathrm{T}}, \mathbf{u}_g^{\mathrm{T}}, u_{\tilde{s}}^{\mathrm{T}}\right]^{\mathrm{T}}$, and $\mathbf{f}$ representing the right-hand side of Eq. (28). The inequality

$$\Delta t_k < \frac{\min\limits_j(z_j - z_{j-1})}{v_s} \tag{30}$$

should be satisfied for sufficiently high accuracy. Here, $\min\limits_j(z_j - z_{j-1})$ denotes the smallest spatial discretization of the strip in the Eulerian reference system. The restriction (30) ensures that each material point in the Lagrangian framework captures the influence (heat flux) of each strip section in the Eulerian framework at least once. Generally, the sampling period Δt_k is critical for the numerical stability of Euler's explicit method. If Eq. (30) is satisfied, stability problems have not been observed with the considered system.

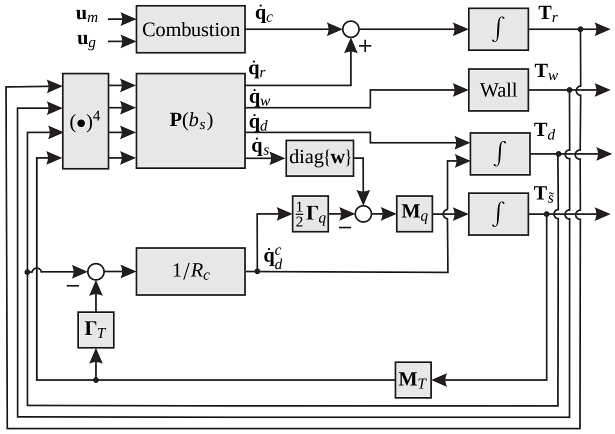

Figure 11: Structure of the mathematical model.

Post-print version of the article: M. Niederer, S. Strommer, A. Steinboeck, and A. Kugi, "A simple control-oriented model of an indirect-fired strip annealing furnace", *International Journal of Heat and Mass Transfer*, vol. 78, pp. 557–570, 2014. DOI: 10.1016/j.ijheatmasstransfer.2014.06.080
The content of this post-print version is identical to the published paper but without the publisher's final layout or copy editing.

2.7. Numerical analysis

To analyze the numerical uncertainty of the developed furnace model (29), the grid convergence index (GCI) [40] is employed. It is based on the generalized theory of the Richardson extrapolation [38, 39] and is commonly used in grid refinement studies.

In order to compute the grid convergence index, at least three different simulations with three different grids with step sizes h_1, h_2, and h_3 are required. These step sizes represent a fine, a medium, and a coarse mesh resolution of the spatial and the temporal discretization, i.e., $h_1 < h_2 < h_3$. Let ϕ_1, ϕ_2, and ϕ_3 be the solutions of a quantity ϕ from the discretized models. The grid convergence index provides an error band for the solution ϕ_1 and is defined as

$$\mathrm{GCI}_{12} = 3\frac{e_{12}}{r^p - 1},$$

where $e_{12} = (\phi_2 - \phi_1)/\phi_1$ is the relative error, $r = h_2/h_1 = h_3/h_2$ is the grid refinement ratio, and p is the formal order of accuracy which can be computed using

$$p = \frac{\log\left((\phi_3 - \phi_2)/(\phi_2 - \phi_1)\right)}{\log(r)}.$$

The most important output of the numerical model is the temperature profile of the strip. For this quantity, the influence of the spatial and temporal discretization on the model accuracy is studied by means of the grid convergence indices GCI_{12}^{RTH} and GCI_{12}^{RTS} for two representative strip elements at the end of the two furnace sections RTH and RTS. Inside the furnace, the spatial discretization is more or less predefined by the structure of the furnace. Both the radiant tubes and the deflection rolls are modeled as discrete elements. A further refinement is thus not useful, i.e., a fixed spatial discretization is used for the radiant tubes and rolls. For determining the grid convergence indices, the spatial and the temporal discretization of the furnace model is refined with a refinement ratio $r = 2$. The required simulations are performed with different strip parameters and input data from the real furnace. In Fig. 12, both the simulated temperature trajectories and the calculated grid convergence indices for the considered strip elements are shown. The scattering of the results is due to the mapping between the Lagrangian and the Eulerian coordinate framework, cf. Sec. 2.3. These results confirm that the temperature error of the considered strip elements due to the discretization does not exceed 1.4% for the considered strip elements of the fine grid. Thus, the chosen discretization seems to be adequate for the proposed application of the furnace model.

3. Example problem

For verification of the model with measurement data, a measurement campaign was conducted at the real plant. For this purpose, the measurement equipment already installed was utilized. In normal furnace operation, the strip temperature, which is of major interest, is measured by means of three radiation pyrometers. The first pyrometer is located at the entry of the furnace (just after the air lock), and its reading is an input of the furnace model. The two other pyrometers P_{RTH} and P_{RTS} are located at the transition between the two furnace sections RTH and RTS, and at the end of the furnace, see Fig. 1. Furthermore, temperatures of some radiant tubes and wall segments are measured by means of thermocouples. The remaining system inputs, i.e., the mass flow of fuel to the control zones and the exhaust gas temperatures of some radiant tubes, are also known from measurements.

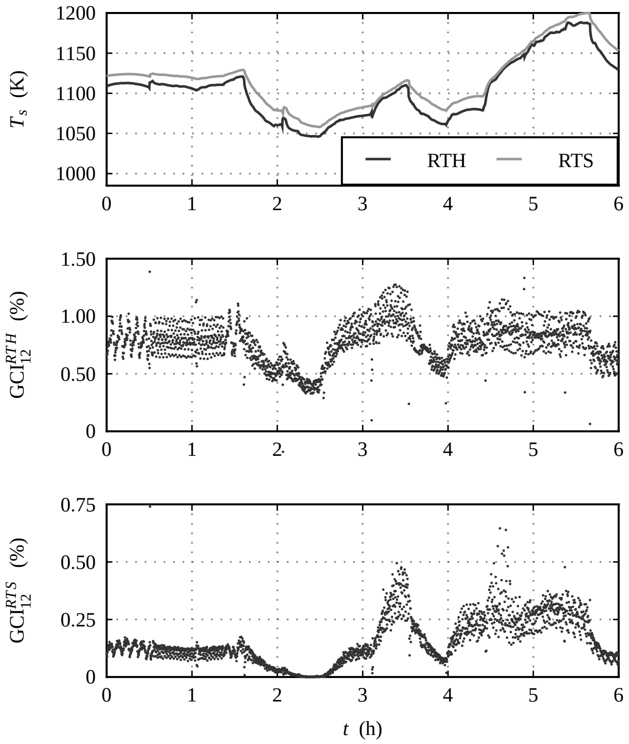

Figure 12: Simulated strip temperature of the fine grid and grid convergence indices for two strip elements at the end of the furnace sections RTH and RTS.

An important output of the model is the temperature of the strip at the pyrometer positions. Its temperature evolution is also determined by the material parameters, i.e., the specific heat capacity and the emissivity. In a radiation pyrometer, the radiative energy $I_p = \sigma\varepsilon_s T_s^4$ incident on its detector is measured. Generally, the emissivity ε_s of the strip must be known and stored in the pyrometer for a correct measurement of the strip temperature T_s. However, unknown radiative properties of the strip could cause measurement errors [10, 42]. Since the emissivity ε_s is both uncertain and difficult to determine, it is a good choice for parameter identification, in particular because the remaining physical parameters in Eq. (28) are at least roughly known from design drawings or material handbooks. In this work, an average strip emissivity $\hat{\varepsilon}_s$ is identified and used for all products. The value $\hat{\varepsilon}_s$ was identified to achieve an optimum match between the temperature $\hat{T}_s = \sqrt[4]{I_p/\sigma\hat{\varepsilon}_s}$ and its simulated counterpart T_s.

During the considered measurement campaign, 42 different products were processed. Within this campaign, the strip ve-

Post-print version of the article: M. Niederer, S. Strommer, A. Steinboeck, and A. Kugi, "A simple control-oriented model of an indirect-fired strip annealing furnace", *International Journal of Heat and Mass Transfer*, vol. 78, pp. 557–570, 2014. DOI: 10.1016/j.ijheatmasstransfer.2014.06.080

locity varies in the range $v_s \in [1.4, 2.8]$ m/s, the width is in the range $b_s \in [0.9, 1.6]$ m, and the thickness $d_s \in [0.5, 1.1]$ mm. Figure 13 shows the measured and simulated strip temperatures at the two pyrometer positions P_{RTH} and P_{RTS}. As it can be inferred from Fig. 13, the temperature evolution of the strip is captured in a very good way by the furnace model and the error between measurements and simulated results is within ±20 K. The accuracy may be further improved by a more detailed specification of the specific heat capacity of the strip and by an online-identification of the emissivity ε_s of the strip. In the considered scenario, the heat capacity of the strip plays an important role since the strip is annealed in a temperature range that contains a phase transition of the material, which significantly influences the temperature evolution of the strip.

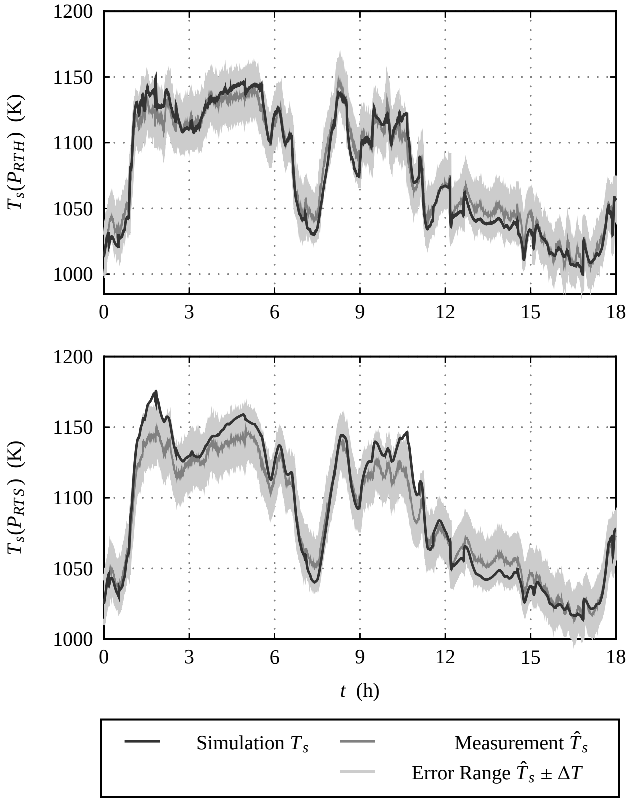

Figure 13: Temperature of the strip at the pyrometer positions P_{RTH} and P_{RTS}.

To further illustrate the accuracy of the numerical results of the strip temperature, an error analysis is performed for the experimental results measured by the pyrometers. If the emissivity of the strip is exactly known, the manufacturer guarantees that the temperature measurement error is less than $\Delta T_m = 4$ K. As mentioned before, the emissivity of the strip is fairly uncertain. When measuring the strip temperature, this causes an additional measurement error ΔT_ε. By introducing the relative emissivity error $\delta = (\hat{\varepsilon}_s - \varepsilon_s)/\hat{\varepsilon}_s$, the measurement error ΔT_ε reads as $\Delta T_\varepsilon = \hat{T}_s(1 - 1/\sqrt[4]{1-\delta})$. Because of the uncertainties of the emissivity and the wide range of different processed products, a relative emissivity error $\delta = \pm 0.05$ is realistic [27, 46]. The pyrometer measurement can also be affected by the surrounding walls. However, the pyrometer is mounted inside a gas cooled pipe that is directed onto the strip surface. This pipe acts as a radiation shield. Hence, the effect of surrounding walls on the measurement can be neglected. Thus, the total temperature measurement error reads as $\Delta T = \Delta T_m + \Delta T_\varepsilon$. Figure 13 also depicts the error range $\hat{T}_s \pm \Delta T$ of the calculated strip temperature from the measurement readings of the pyrometers and the simulated strip temperatures. It can be deduced that the simulated strip temperatures are within the error range of the pyrometers, which demonstrates once again the high accuracy of the developed furnace model.

In Fig. 14, the temperature trajectory of a strip point is shown as it moves through the furnace. The figure reveals the essential purposes of the furnace sections RTH and RTS. In the first section, the preheated strip is further heated, whereas the temperature is just kept on a desired level in the second section. In addition, the figure indicates the influence of the deflection rolls in the form of short temperature plateaus.

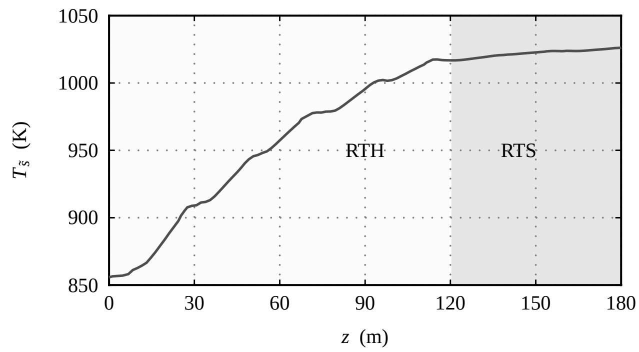

Figure 14: Simulated temperature profile of a processed strip section.

The temperatures of a radiant tube T_r and a wall segment T_w are shown in Fig. 15. Again the simulated results match well with the measurements.

The mathematical model was implemented and simulated on a standard desktop PC (3.6 GHz, 4 GB RAM) with an equidistant sampling rate $\Delta t_k = 100$ ms. On this computer, 1 h furnace operation needs approximately 160 s CPU-time for simulation. This result makes sure that the derived model is suitable for real-time applications in control and optimization. If a variable sampling rate which always satisfies condition (30) is used, the simulation time can be further reduced without a significant loss of accuracy. The furnace model is currently used as an add-on device for permanent online monitoring of process variables that cannot be measured. This application of the proposed model provides the furnace operators with new insight into the annealing process and thus helps to further increase the product quality and the throughput.

4. Conclusions

A mathematical model of an indirect-fired strip annealing furnace was derived. The focus of research was to obtain a first-principles model that includes the essential nonlinearities

Post-print version of the article: M. Niederer, S. Strommer, A. Steinboeck, and A. Kugi, "A simple control-oriented model of an indirect-fired strip annealing furnace", *International Journal of Heat and Mass Transfer*, vol. 78, pp. 557–570, 2014. DOI: 10.1016/j.ijheatmasstransfer.2014.06.080
The content of this post-print version is identical to the published paper but without the publisher's final layout or copy editing.

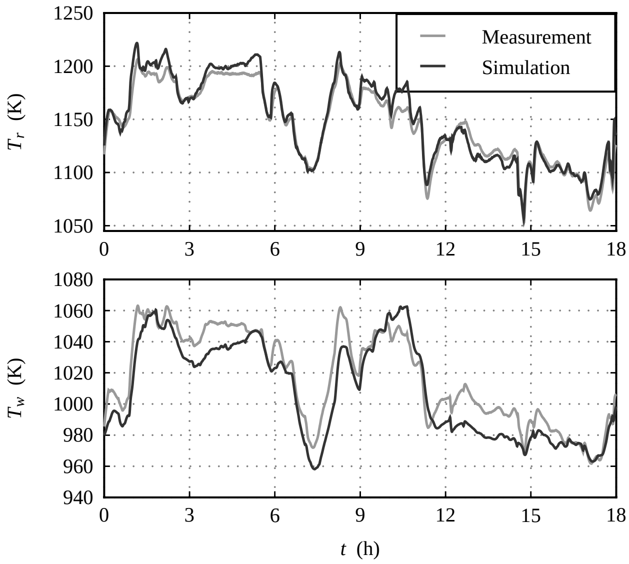

Figure 15: Temperatures of a radiant tube T_r and a wall segment T_w.

of the system and that is suitable for control and real-time optimization applications.

In order to model the heat conduction through the multi-layered furnace wall, the corresponding 1-dimensional heat conduction equation was discretized by means of the Galerkin weighted residual method. To achieve a high accuracy of the model, the stationary solution of the heat conduction equation was used as trial function. The combustion of natural gas takes place inside the radiant tubes. The released heat is transferred by heat conduction through the tubes to the furnace interior and was calculated by means of steady-state mass and energy balances. For each tube, the 1-dimensional heat conduction equation was again approximated by using the Galerkin method. The heat transferred to the furnace is mainly used to heat the strip to a desired temperature. The strip temperature was described by a simple heat balance in the Lagrangian reference system, which is especially useful for capturing the temperature transition at welded joints between consecutive strips. Furthermore, the deflection rolls were modeled as lumped parameter systems by using simple heat balances. The coupling of all submodels was considered by means of heat conduction and radiation. For calculating the radiative heat transfer, the net radiation method was employed.

The main advantage of the derived furnace model is that it constitutes a good tradeoff between accuracy and computational efficiency. Moreover, the model covers the most important nonlinear effects, i.e., the combustion of natural gas, the heat transfer by radiation, and the temperature dependence of material parameters.

Acknowledgements

This research was partially supported by the Austrian Research Promotion Agency (FFG), Grant No.: 834305. Moreover, the authors are grateful to the industrial research partners voestalpine Stahl GmbH and Andritz AG. The third author gratefully acknowledges financial support provided by the Austrian Academy of Sciences in the form of an APART-fellowship at the Automation and Control Institute of Vienna University of Technology.

References

[1] M. Ahanj, M. Rahimi, and A. Alsairafi. CFD modeling of a radiant tube heater. *International Communications in Heat and Mass Transfer*, 39(3):432 – 438, 2012.

[2] H.D. Baehr and K. Stephan. *Heat and Mass Transfer*. Springer, Berlin, Heidelberg, 2nd edition, 2006.

[3] H.J. Bargel and G. Schulze. *Werkstoffkunde*. Springer, Berlin, Heidelberg, 9th edition, 2005.

[4] K. Bathe. *Finite-Elemente-Methoden*. Springer, Berlin, Heidelberg, 2nd edition, 2002.

[5] L. Bitschnau and M. Kozek. Modeling and control of an industrial continuous furnace. In *Proceedings of the CSSim 2009 Computational Intelligence, Modelling and Simulation Conference, Brno, Czech Republic*, pages 231–236, September 2009.

[6] P. Boineau, C. Copin, and F. Aguile. Heat transfer modelling using advanced zone model base on a CFD code. In *Proceedings of the Modélisation du rayonnement et simulation numérique des fours*, pages A1–A11, Paris, France, May 2002.

[7] L. Bordignon, G. Angeli, H. Bolt, R. Hekkens, W. Maschek, J. Paavilainen, and X.V. Eynde. Enhanced Hot Dip Galvanising by Controlled Oxidation in the Annealing Furnace. In *Proceedings of the 44th Mechanical Working and Steel Processing Conference (MWSP)*, volume XL, pages 833–844, Orlando, USA, September 2002.

[8] S.R. Carvalho, T.H. Ong, and G. Guimarães. A mathematical and computational model of furnaces for continuous steel strip processing. *Journal of Materials Processing Technology*, 178:379–387, 2006.

[9] T.-C. Chen, C.-H. Ho, J.-. Lin, and L.-W. Wu. 3-D temperature and stress distributions of strip in preheating furnace of continuous annealing line. *Applied Thermal Engineering*, 30:1047–1057, 2010.

[10] R.R Corwin and A. Rodenburgh II. Temperature error in radiation thermometry caused by emissivity and reflectance measurement error. *Applied Optics*, 33(10):1950–1957, 1994.

[11] N. Depree, J. Sneyd, S. Taylor, M.P. Taylor, J.J.J. Chen, S. Wang, and M. O'Connor. Development and validation of models for annealing furnace control from heat transfer fundamentals. *Journal of Computers and Chemical Engineering*, 34:1849–1853, 2010.

[12] G. Fairweather. *Finite Element Galerkin Methods for Differential Equations*, volume 34 of *Lecture notes in pure and applied mathematics*. M. Dekker, Inc., New York, 1978.

[13] C.A.J. Fletcher. *Computational Galerkin Method*. Springer, Berlin, Heidelberg, 1984.

[14] F. Hollander and S.P.A. Zuurbier. Design, development and performance of online computer control in a 3-zone reheating furnace. *Iron and Steel Engineer*, 59(1):44–52, 1982.

[15] J.P. Holman. *Heat Transfer*. McGraw-Hill, New York, 10th edition, 2010.

[16] H.C. Hottel. Radiant-Heat transmission. In W.H. McAdams, editor, *Heat Transmission*, chapter 4. McGraw-Hill, New York, 3rd edition, 1954.

[17] H.C. Hottel and E.S. Cohen. Radiant heat exchange in a gas filled enclosure: Allowance for non-uniformity of gas temperature. *American Institute of Chemical Engineering Journal*, 4:3–14, 1958.

[18] H.C. Hottel and A.F. Sarofim. *Radiative Transfer*. McGraw-Hill, New York, 1967.

[19] F.P. Incropera, D.P. DeWitt, T.L. Bergman, and A.S. Lavine. *Fundamentals of Heat and Mass Transfer*. John Wiley & Sons, Hoboken, New Jersey, 6th edition, 2007.

[20] M. Irfan and W. Chapman. Thermal stresses in radiant tubes: A comparison between recuperative and regenerative systems. *Applied Thermal Engineering*, 30:196–200, 2010.

[21] J. H. Lienhard IV and J. H. Lienhard V. *A Heat Transfer Textbook*. Phlogiston Press, Cambridge, Massachusetts, USA, 3rd edition, 2008.

[22] C.D. Kelly, D. Watanapongse, and K.M. Gaskey. Application of modern control to a continuous anneal line. *IEEE Control Systems Magazine*, 8(2):32–37, April 1988.

Post-print version of the article: M. Niederer, S. Strommer, A. Steinboeck, and A. Kugi, "A simple control-oriented model of an indirect-fired strip annealing furnace", *International Journal of Heat and Mass Transfer*, vol. 78, pp. 557–570, 2014. DOI: 10.1016/j.ijheatmasstransfer.2014.06.080
The content of this post-print version is identical to the published paper but without the publisher's final layout or copy editing.

[23] P. Kokotovic, H.K. Khalil, and J. O'Reilly. *Singular perturbation methods in control*. Society for Industrial and Applied Mathematics, Philadelphia, 1999.

[24] F. Kreith. *The CRC Handbook of Thermal Engineering*. CRC Press, Boca Raton, 1999.

[25] D. Marlow. *Mathematical modelling of the heat treatment in the continuous processing of steel strip*. PhD thesis, University of Wollongong, Australia, 1995.

[26] M. McGuinnes and S. Taylor. Strip temperature in a metal coating line annealing furnace. Technical report, Mathematics in Industry, 2004. `http://www.math.auckland.ac.nz/deptdb/dept_reports/532.pdf`.

[27] L. Michalski, K. Eckersdorf, J. Kucharski, and J. McGhee. *Temperature Measurement*. John Wiley & Sons, Hoboken, New Jersey, 2^{nd} edition, 2001.

[28] Z. Ming, Y. Datai, and Z. Jiangang. A new strip temperature control method for the heating section of continuous annealing line. In *Proceedings of the IEEE 2008 Conference on Cybernetics and Intelligent Systems*, pages 861–864, Chengdu, China, September 2008.

[29] A. Mochida, K. Kudo, Y. Mizutani, M. Hattori, and Y. Nakamura. Transient heat transfer analysis in vacuum furnaces heated by radiant tube burners. *Energy Conversion and Management*, 38(10-13):1169 – 1176, 1997.

[30] M.F. Modest. *Radiative Heat Transfer*. Academic Press, San Diego, 2^{nd} edition, 2003.

[31] M.J. Moran and H.N. Shapiro. *Fundamentals of Engineering Thermodynamics*. John Wiley & Sons, New York, 6^{th} edition, 2010.

[32] M. Niederer, A. Steinböck, S. Strommer, and A. Kugi. Analysis of radiative heat transfer in an indirect-fired strip annealing furnace based on integral equations. In *Proceedings of 15th IFAC Symposium on Control, Optimization and Automation in Mining, Mineral & Metal Processing*, pages 403–408, San Diego, USA, 2013.

[33] M. Niederer, A. Steinböck, S. Strommer, and A. Kugi. Control of radiant tubes in an indirect-fired strip annealing furnace for improved efficiency. In *Proceedings of European Control Conference ECC 2013*, pages 1–6, Zurich, Switzerland, 2013.

[34] M.N. Oezisik. *Finite Difference Methods in Heat Transfer*. CRC Press, Boca Raton, 1994.

[35] B.E. Poling, J.M. Prausnitz, and J.P. O'Connell. *The Properties of Gases and Liquids*. McGraw-Hill, New York, 5^{th} edition, 2004.

[36] H. Ramamurthy, S. Ramadhyani, and R. Viskanta. A thermal system model for a radiant-tube continuous reheating furnace. *Journal of Materials Engineering and Performance*, 4(5):519–531, 1995.

[37] H. Ramamurthy, S. Ramadhyani, and R. Viskanta. Development of fuel burn-up and wall heat transfer correlations for flows in radiant tubes. *Numerical Heat Transfer, Part A*, 31:563–584, 1997.

[38] L.F. Richardson. The approximate arithmetical solution by finite differences of physical problems involving differential equations, with an application to the stresses in a masonry dam. *Transactions of the Royal Society of London*, 210:307–357, 1910.

[39] L.F. Richardson and J.A. Gaunt. The deferred approach to the limit. *Transactions of the Royal Society of London*, 226:299–361, 1927.

[40] P.J. Roache. Perspective: A method for uniform reporting of grid refinement studies. *Journal of Fluids Engineering*, 116:405–413, 1994.

[41] R. Siegel and J. Howell. *Thermal Radiation Heat Transfer*. Taylor and Francis, New York, 4^{th} edition, 2002.

[42] K. Speicher, A. Steinböck, D. Wild, T. Kiefer, and A. Kugi. Measurement errors of radiation pyrometers and their corrections. In *Proceedings of the 9^{th} International Rolling Conference*, pages 1–12, Venice, Italy, 2013.

[43] S. Strommer, M. Niederer, S. Steinboeck, and A. Kugi. A mathematical model of a direct-fired continuous strip annealing furnace. *International Journal of Heat and Mass Transfer*, 69:375–389, 2014.

[44] J.W. Thomas. *Numerical Partial Differential Equations: Finite Difference Method*. Springer, New York, 1995.

[45] Y.-C. Tian, C.-H. Hou, and F. Gao. Mathematical model of a continuous galvanizing annealing furnace. *Developments in Chemical Engineering and Mineral Processing*, 8(3–4):359–374, 2000.

[46] Y.S. Touloukian and D.P. DeWitt. *Thermophysical Properties of Matter - The TPRC Data Series. Volume 7. Thermal Radiative Properties - Metallic Elements and Alloys*. Defense Technical Information Center, 1970.

[47] S.R. Turns. *An Introduction to Combustion: Concepts and Applications*. McGraw-Hill, New York, 2^{nd} edition, 2006.

[48] N. Yoshitani. Modeling and parameter estimation for strip temperature control in continuous annealing processes. In *Proceedings of the International Conference on Industrial Electronics, Control, and Instrumentation (IECON)*, volume 1, pages 469–474, Maui, November 1993.

[49] O.C. Zienkiewicz and K. Morgan. *Finite Elements and Approximation*. John Wiley & Sons, Hoboken, New Jersey, 1^{st} edition, 1983.

[50] O.C. Zienkiewicz, R.L. Taylor, and J.Z. Zhu. *The Finite Element Method: Its Basis and Fundamentals*. Elsevier, 6^{th} edition, 2005.

Post-print version of the article: M. Niederer, S. Strommer, A. Steinboeck, and A. Kugi, "A simple control-oriented model of an indirect-fired strip annealing furnace", *International Journal of Heat and Mass Transfer*, vol. 78, pp. 557–570, 2014. DOI: 10.1016/j.ijheatmasstransfer.2014.06.080
The content of this post-print version is identical to the published paper but without the publisher's final layout or copy editing.